


Split-design approach enhances the therapeutic efficacy of ligand-based CAR-T cells against multiple B-cell malignancies

Received: 18 January 2024

Accepted: 2 November 2024

Published online: 11 November 2024

 Check for updates

Shuhong Li¹, Licai Shi¹, Lijun Zhao¹, Qiaoru Guo¹, Jun Li², Ze-lin Liu³, Zhi Guo³ & Yu J. Cao^{1,4} 

To address immune escape, multi-specific CAR-T-cell strategies use natural ligands that specifically bind multiple receptors on malignant cells. In this context, we propose a split CAR design comprising a universal receptor expressed on T cells and ligand-based switch molecules, which preserves the natural trimeric structure of ligands like APRIL and BAFF. Following optimization of the hinges and switch labeling sites, the split-design CAR-T cells ensure the native conformation of ligands, facilitating the optimal formation of immune synapses between target cancer cells and CAR-T cells. Our CAR-T-cell strategy demonstrates antitumor activities against various B-cell malignancy models in female mice, potentially preventing immune escape following conventional CAR-T-cell therapies in the case of antigen loss or switching. This ligand-based split CAR design introduces an idea for optimizing CAR recognition, enhancing efficacy and potentially improving safety in clinical translation, and may be broadly applicable to cellular therapies based on natural receptors or ligands.

Despite substantial advances in improving patient outcomes, chimeric antigen receptor (CAR)-T-cell therapy still faces the challenge of relapse. A considerable portion of these cases involve the loss of the target antigen¹. Although various bispecific CAR-T-cell strategies, such as CD19/CD20 or CD19/CD22 CAR-T-cell therapy for B-cell leukemia (B-ALL)^{2,3}, and BCMA/CD38 or CS1/BCMA CAR-T-cell therapy for multiple myeloma (MM)^{4,5}, have been developed, the sequential loss of dual antigens when coadministering CAR-T cells has also been reported⁶. To address this challenge, trispecific CAR-T cells targeting tumor cells utilizing the duoCAR format with scFvs have been proposed⁷. However, these approaches carry the potential risk of chain mispairing, leading to CAR aggregation and triggering T-cell-exhausting signaling cascades⁸.

Alternatively, CAR designs incorporating natural ligands or receptor ectodomains, which inherently bind to multiple markers on

malignant cells, present a potential solution for antigen escape. A proliferation-inducing ligand (APRIL) and B-cell activating factor (BAFF), both of which are members of the TNF ligand superfamily, have been integrated into CAR designs to target multiple receptors, including BAFFR, BCMA and TACI^{9,10}, in attempts to prevent antigen escape. Preclinical studies have demonstrated the effectiveness of APRIL- or BAFF-based CAR-T-cell approaches in eradicating various B-cell cancers and maintaining antitumor functions even in response to the loss of the BCMA or CD19 antigen^{11–15}. Recognizing the essential trimeric format of both ligands, significant efforts have been directed toward preserving their natural conformation anchored on the cell membrane to enhance their binding and efficacy against target cells^{13,16}. The use of the 4-1BB transmembrane domain to promote multimerization of the trimeric APRIL ligand on the cell membrane has been reported, with superior therapeutic effects compared with the

¹State Key Laboratory of Chemical Oncogenomics, Shenzhen Key Laboratory of Chemical Genomics, Peking University Shenzhen Graduate School, Shenzhen, Guangdong, China. ²Fundamenta Therapeutics Co., Ltd, Suzhou, Jiangsu, China. ³Department of Hematology, Huazhong University of Science and Technology Union Shenzhen Hospital (Nanshan Hospital), Shenzhen, Guangdong, China. ⁴Institute of Chemical Biology, Shenzhen Bay Laboratory, Shenzhen, China. ✉e-mail: joshuacao@pku.edu.cn

monomeric APRIL format¹⁴. Nevertheless, researchers have not yet determined the comparative efficacy of these modified ligands relative to their natural soluble counterparts.

The switchable CAR-T (sCAR-T)-cell platform comprises a universal receptor expressed on T cells and a tumor-targeting adapter molecule^{17–19}. This platform features a unique split CAR design with the potential to confer strong natural properties on target ligands²⁰. By expanding the sCAR-T-cell strategy, our group and others have explored the flexibility of simultaneously designing the sCAR hinge and switch labeling sites to achieve optimal distance and orientation for CAR-T-cell activation^{17,18}. The sCAR-T-cell platform modularizes CAR-T cells, providing enhanced flexibility in clinical oncology treatment. Moreover, this strategy allows dose-titratable control of sCAR-T-cell activity, addressing safety concerns associated with conventional CAR-T cells¹⁹. Notably, the risk of normal tissue toxicity increases when tumor-associated antigens (TAAs) are targeted with APRIL- or BAFF-based CAR-T cells. Therefore, designing sCAR-T cells utilizing natural ligands is highly desirable for maintaining their optimal structures and functionalities while minimizing the potential for serious treatment-related toxicity.

In this work, we introduce a sCAR strategy for ligand-mediated CAR-T-cell activation in which split APRIL- or BAFF-based switches are designed to maintain their native structures, resulting in a highly sensitive response to multiple targets in B-cell malignancies. Through the optimization of switch architecture and CAR hinge design, APRIL- and BAFF-based sCAR-T cells promote optimal synapse formation between target cells and effector cells, leading to enhanced cytokine production and excellent antitumor efficacy against various B-cell malignancies both *in vitro* and *in vivo*. Recognizing the potential of immune escape due to antigen loss, we assess the effectiveness of ligand-based sCAR-T cells in the context of heterogeneous malignancies lacking multiple B-cell markers and demonstrate overall enhanced tumor growth inhibition compared with previously reported CAR-T-cell approaches. Notably, our sCAR strategy exhibits therapeutic efficacy comparable to FDA-approved therapies. In summary, we propose a sCAR-T-cell approach based on APRIL and BAFF that is characterized by an optimal synergistic structural design that enhances the functionality of natural ligands, potentially overcoming the limitations of conventional CAR structures with restricted target specificity.

Results

Design and characterization of APRIL- and BAFF-based switches

Building upon the inherent multireceptor specificity of natural ligands, we expanded the sCAR-T-cell platforms introduced previously^{17,18} using APRIL- or BAFF-based switches. Flow cytometry analysis confirmed the expression of BAFFR, BCMA, and TACI in a range of B-cell malignancies (Supplementary Fig. 1 and Supplementary Table 1). Subsequently, we introduced a 10-aa peptide derived from Myc (EQKLISEEDL) at the N- or C-terminus of the extracellular domains of APRIL and BAFF, creating four constructs: Myc-APRIL, APRIL-Myc, Myc-BAFF and BAFF-Myc (Fig. 1a). These proteins were purified to greater than 95% purity, as confirmed by SDS-PAGE (Supplementary Fig. 2). Size exclusion chromatography analysis verified the presence of four switch fusions in trimeric forms, without any multimeric aggregation (Supplementary Fig. 3 and Supplementary Table 2–3). The binding assay revealed that the two APRIL switches exhibited similar binding profiles to the BCMA and TACI antigens; however, compared with Myc-BAFF, BAFF-Myc exhibited reduced antigen binding activity (Fig. 1b). When exposed to 100 nM fusion proteins, both BAFF switches bound to tumor cells to a similar extent; nonetheless, APRIL-Myc exhibited nonspecific binding, in contrast to Myc-APRIL (Supplementary Fig. 4a).

For switch comparison, we used sCAR-T cells harboring the IgG4m hinge derived from a dimeric mutant (S228P) of the IgG4

hinge¹⁸, which we have previously shown to outperform other hinge designs. The immunological synapse (IS) is a precise structure that is formed between T cells and target cells through receptor–ligand interactions to perform the immunological function of T cells²¹. The quality of the IS²² serves as a reliable predictor of the efficacy of CAR-modified cells and can be correlated with clinical outcomes²¹. PKC- θ , the most abundant protein kinase C (PKC) in hematopoietic cells, is the only PKC isoform that is selectively recruited to the IS in conventional effector T (T_{eff}) cells²³. Therefore, evaluating the strength of the PKC- θ polarization signal at immune synapses is helpful for measuring the strength of immune synapses and identifying the best CAR candidate molecules. As illustrated in Figs. 1c, d, both Myc-APRIL and Myc-BAFF promoted more efficient IS formation, and fluorescence quantification confirmed their ability to increase downstream signal transduction (Figs. 1e, f). Cytotoxicity assays (Figs. 1g, h) revealed that placing both Myc-fusion switches at the N-terminus induced more pronounced lysis of target cells than fusing Myc at the C-terminus across various cell lines. Analysis of proinflammatory cytokine secretion further supported these findings (Supplementary Fig. 4b). Therefore, we propose that APRIL- and BAFF-based switches featuring the Myc fusion site at the N-terminus provide optimal specificity. These switches exhibit high-specificity binding to various B-cell malignancies, supporting a multitargeting approach against two or three antigens.

Optimal design of switchable CAR-T cells

It has been reported that using a hinge region of suitable length is essential for achieving the appropriate intercellular distance for optimal IS formation^{24,25}. Thus, we conducted hinge optimization of Myc-specific CARs by testing three hinges of different lengths (Fig. 2a). The lentiviral transduction of the three constructs resulted in similar surface expression efficiencies (Supplementary Fig. 5b). As shown in Fig. 2b–c, 9E10-IgG4m CAR-T cells promoted significantly stronger IS formation with RPMI8226 than others in the presence of Myc-APRIL. Similarly, during IS formation with Nalm6, 9E10-IgG4m CAR-T cells exhibited notably stronger PKC- θ fluorescence signals in the presence of Myc-BAFF than the other two CAR-T-cell candidates (Fig. 2d–e). Moreover, 9E10-IgG4m CAR-T cells with Myc-APRIL induced stronger cytotoxicity against MM cells (Fig. 2f). Additionally, Myc-BAFF significantly enhanced the antigen-specific cytotoxicity of 9E10-IgG4m CAR-T cells compared to that of other CAR-T cells (Fig. 2g), indicating its broad potential for targeted killing of B-cell malignancies. Furthermore, 9E10-IgG4m CAR-T cells induced significantly greater cytokine secretion in the presence of either Myc-APRIL or Myc-BAFF (Fig. 2h–i). We hypothesized that a shorter hinge length would be more conducive to the function of sCAR-T cells, possibly because the free switches ensure an optimal antigen-binding conformation, and the short hinge length accelerates signaling. To validate this, we assessed cytotoxicity at lower E:T ratios or switch concentrations. As shown in Fig. 2j–k, Supplementary Fig. 6a–b, both APRIL- and BAFF-redirected sCAR-T cells demonstrated excellent and broad-spectrum cytotoxicity under these conditions, confirming the enormous clinical potential of this system. Additionally, stable dimerized formation, but not trimerization or aggregation, of CAR molecules was observed in 9E10-IgG4m CAR-T cells, regardless of the switch concentration (Supplementary Fig. 7). Taken together, our results indicate that incorporating the IgG4m hinge into anti-Myc CAR-T cells enhances the ligand-mediated interaction between the target and effector cells, thereby improving antigen-specific CAR-T-cell activities.

In vitro comparison of the split-design CAR approach with ligand-based conventional CAR

Because APRIL and BAFF are both type II transmembrane proteins, the immobilization of APRIL- or BAFF-based conventional CARs not only presents challenges in terms of regulating immune strength but also may impair receptor binding activity^{26–28}. To investigate whether

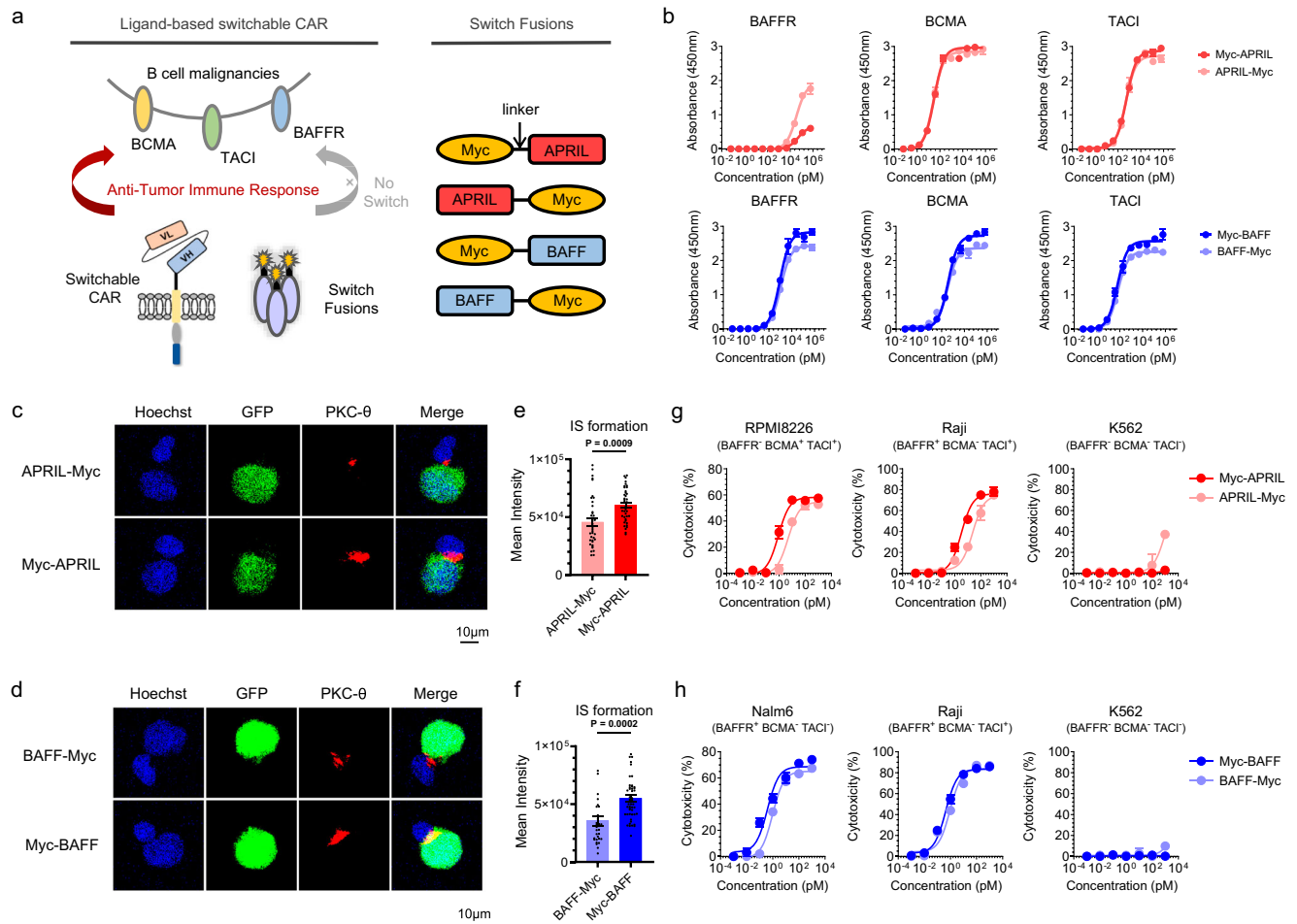
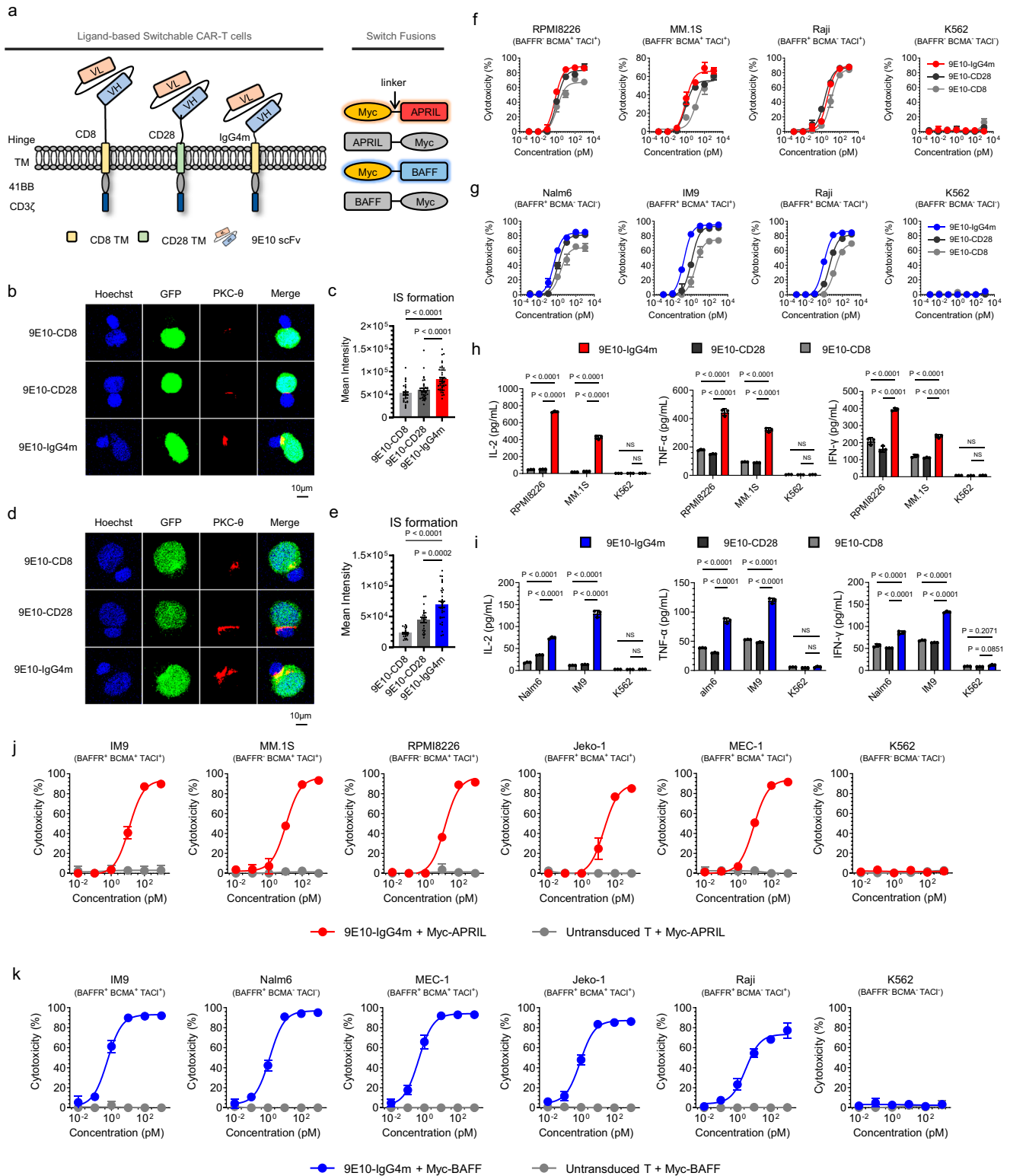


Fig. 1 | Design and comparison of BAFF- and APRIL-based switches. **a** Schematic representation of the ligand-based CAR-T-cell system using a split-design approach. The system comprises Myc-targeted sCAR-T cells and ligand-Myc-based switch fusions, allowing redirection to the B-cell malignant tumor antigens BCMA, TACI and BAFFR. The Myc tag was fused to the N- or C-terminus of the extracellular domain of APRIL or BAFF ligand with a flexible GGGGS linker. Consequently, four switches were generated and referred to as Myc-APRIL, APRIL-Myc, Myc-BAFF and BAFF-Myc. **b** Binding profiles of APRIL- or BAFF-based switches to antigens BAFFR, BCMA, and TACI were determined by ELISA in triplicate. **c, d** Representative confocal images of synapses. sCAR-T cells were co-cultured with RPMI8226-GFP cells in the presence of APRIL-based switches (**c**) or co-cultured with Nalm6-GFP cells in the presence of BAFF-based switches (**d**) for 1 h, and cell-cell conjugates were imaged

at 100 \times oil objective magnification using a laser scanning confocal microscope (Nikon, AIR). Hoechst (blue), anti-PKC- θ (red), GFP (green) and merged images of all the stains are shown. Scale bar=10 μ m. **e, f** Statistical analysis of mean fluorescence intensity of PKC- θ at the IS in the panels (**c**) and (**d**), respectively. Sample sizes: APRIL-Myc/Myc-APRIL, $n = 39$; BAFF-Myc, $n = 31$; Myc-BAFF, $n = 48$. All n values represent individual cells. P values determined by paired two-tailed t -tests. **g, h** Cytotoxicity assays of different APRIL- (**g**) or BAFF-based switches (**h**) were performed with sCAR-T cells against the indicated target cells at an E:T ratio of 10:1 for 24 h in triplicate. Data in this figure are representative of three independent experiments. Error bars represent mean \pm SD. NS indicates not significant. Source data are provided in the Source Data file.

the split design can preserve the activities of natural ligands, we included conventional CAR-T cells as comparative candidates. Conventional CAR-T cells, named APRIL CAR and BAFF CAR, have the same hinge and transmembrane domains described in previous reports^{12,15}, and their intracellular domains are consistent with those of 9E10 CAR-T cells (Fig. 3a and Supplementary Fig. 5a). As shown in Fig. 3b-e, both types of sCAR-T cells led to significantly increased IS formation compared to that of their corresponding conventional CAR-T-cell counterparts. Although there was a slight difference in the cytotoxicity of the two APRIL-based CAR-T cells against MM cells (Fig. 3f and Supplementary Fig. 8a), the assessment of cytokine production suggested that the structural design of the sCAR-T cells redirected by Myc-APRIL was superior to that of the APRIL CAR-T cells for antigen-dependent T-cell activation (Fig. 3h). In the case of BAFF-based CAR, the sCAR-T cells demonstrated significantly stronger cytotoxicity (Fig. 3g and Supplementary Fig. 8b) and induced higher pro-inflammatory cytokine production (Fig. 3i) than conventional BAFF CAR-T cells.

As expected, we observed in vitro that sCAR-T cells enhanced the antitumor activity of APRIL- or BAFF-based conventional CAR-T cells to varying degrees. This prompted us to further validate the superiority of our design on primary patient samples. Subsequently, we conducted antigen profiling of primary tumor cells, including MM, MCL, ALL and CLL/SLL types (Supplementary Table 4). In addition to the notable expression of the BCMA antigen in MM patients, other tumor types exhibited high levels of the BAFFR antigen, and all patients expressed at least one of these antigens (Supplementary Fig. 9). Two APRIL-specific CAR-T cells exhibited comparable cytotoxicity, while conventional BAFF CAR-T cells exhibited poorer activity than split-design CAR-T cells did (Supplementary Figs. 10a, b). Pro-inflammatory cytokine production analysis revealed significant enhancements in sCAR-T cells specific to both APRIL and BAFF compared to conventional designs (Supplementary Figs. 11a, b). Following the co-cubation of primary MM tumor cells with APRIL- or BAFF-based CAR-T cells, it was observed that sCAR-T cells led to increased



secretion of IL-2 and IFN-γ cytokines (Supplementary Fig. 11c). Taken together, our findings suggest that simply anchoring a ligand protein to the cell membrane not only results in conformational changes but also carries the risk of disrupting ligand homotrimerization. This result emphasizes the essential role of the split-design CAR approach in preserving the original binding activities of natural ligands without compromising antitumor activities.

In vitro comparison of the split-design CAR approach with FDA-approved CAR-T-cell therapies

Tisagenlecleucel (CD19 CAR-T) and Ciltacabtagene autoleucel (BCMA CAR-T), established as the gold standards for CAR-T-cell therapy, were included in this study to evaluate the efficacy of the split-design CAR approach (Supplementary Fig. 5, Figs. 3j and l). Initially, we observed that the cytotoxicity of APRIL-based sCAR-T cells was comparable to that of BCMA CAR-T cells in a series of BCMA/TACI double-positive cell

Fig. 2 | Characterization of sCAR-T hinge designs. **a** Schematic representations of different ligand-based sCAR structures. Second-generation sCARs were engineered comprising a Myc-targeted scFv (clone 9E10), a hinge-transmembrane domain (CD8-CD8, CD28-CD28 or IgG4m-CD8) and an intracellular domain (41BB-CD3 ζ), designated as 9E10-CD8, 9E10-CD28 and 9E10-IgG4m, respectively.

b, d Representative images of cell–cell conjugates were acquired at 100 \times oil objective magnification under a laser scanning confocal microscope (Nikon, AIR). sCAR-T cells, as indicated, were pre-incubated with Myc-APRIL or Myc-BAFF and co-cultured with their respective target cells for 1 h. Fluorescent labeling included Hoechst (blue), anti-PKC- θ (red), and GFP (green) and a merged view of all stains. Scale bar = 10 μ m. **c, e** Statistical analysis of the mean fluorescence intensity of PKC- θ at the IS in panels b and d, respectively. In panel c, samples sizes: 9E10-CD8, $n = 28$; 9E10-CD28, $n = 38$; 9E10-IgG4m, $n = 43$. In panel e, 9E10-CD8, $n = 23$; 9E10-

CD28, $n = 22$; 9E10-IgG4m, $n = 32$. All n values represent individual cells. P values were determined by paired two-tailed t -tests. **f, g** Cytotoxicity assays of different sCAR-T cells against the indicated target cells with Myc-APRIL (**f**) or Myc-BAFF (**g**) at an E:T ratio of 10:1 for 24 h in triplicate. **h, i** Inflammatory cytokine release assay. sCAR-T cells were co-cultured with the specified target cells in the presence of 100 pM Myc-APRIL (**h**) or Myc-BAFF (**i**) for 24 h at an E:T ratio of 1:1 in triplicate. Two-way ANOVA multiple comparisons in Dunnett correction were used to assess significance. **j, k** Cytotoxicity assays of 9E10-IgG4m CAR-T cells against the indicated target cells with Myc-APRIL (**j**) or Myc-BAFF (**k**) at an E:T ratio of 1:1 for 24 h in triplicate. Data in this figure are representative of three independent experiments. Error bars represent mean \pm SD. NS indicates not significant. Source data are provided in the Source Data file.

ligands with clinically relevant antigen densities (Fig. 3k, Supplementary Fig. 12a). To further explore APRIL's potential as a BCMA targeting domain, we generated BCMA-expressing cell lines with gradient densities (Supplementary Fig. 12b), covering the range observed in patient samples (Supplementary Fig. 12c). The killing activity of APRIL-redirected sCAR-T cells was consistent with that of BCMA-CAR-T cells in cell lines with medium-to-high antigen densities but was slightly reduced in cell lines with low BCMA expression (Supplementary Fig. 12d). This difference may be attributed to the ability of BCMA CAR-T cells to target two epitopes of the BCMA antigen simultaneously²⁹. By comparing BAFF-redirected sCAR-T cells with CD19 CAR-T cells, we observed similar killing activity in the BAFFR/BCMA/TACI triple-positive IM9 cell line but inferior activity in other cell lines with clinically relevant antigen densities (Fig. 3m, Supplementary Fig. 12e and g). This disparity is likely due to the significantly lower density of BAFFR/BCMA/TACI antigens than of CD19 antigens (Supplementary Fig. 12f). However, it is noteworthy that although the efficacy of BAFF-specific sCAR-T cells is inferior to that of CD19 CAR-T cells in these contexts, BAFF-specific sCAR-T cells have advantages in cell lines lacking CD19 targets (Fig. 3m), highlighting the strength of BAFF as a targeting domain in hematological tumors, particularly its ability to overcome CD19 antigen escape. In summary, while sCAR-T cells show a gap in single-target capability compared with FDA-approved therapies, the multi-targeting ability and flexibility of the split-design CAR approach provide advantages and significant clinical translational potential.

Sensitivity and controllability of split-design ligand-based CAR-T cells in vivo

To evaluate the in vivo antitumor activity of sCAR-T cells, we utilized RPMI8226 (MM) and Nalm6 (B-ALL) xenograft models for stress testing. Despite the short half-life of switch fusions in mice, typically 20–30 minutes, as previously reported³⁰ (Supplementary Figs. 13a, b), IRDye800-labeled Myc-APRIL and Myc-BAFF remained detectable in tumors up to 48 h post-administration in s.c. tumor-bearing mice (Supplementary Figs. 13c, d). For APRIL-redirected sCAR-T cells, adjustments in both the CAR-T and switch dosages effectively eliminated or inhibited tumor growth, with higher doses leading to faster and more complete tumor clearance (Supplementary Figs. 14a–c). Serum cytokine release was positively correlated with dosage at 24 h post-administration (Supplementary Fig. 14d). Importantly, no significant weight loss was observed in the treated mice throughout the experiment (Supplementary Fig. 14e), and all the treatment groups showed significantly prolonged survival (Supplementary Fig. 14f). Similar outcomes were observed with BAFF-based sCAR-T-cell therapy. Tumor recurrence rates were influenced by alterations in the sCAR-T and switch dosages (Supplementary Fig. 15a–c). In vivo cytokine release was finely regulated in response to dosage adjustments (Supplementary Fig. 15d), maintaining controllable side effects, with varying degrees of prolonged mouse survival (Supplementary Fig. 15e–f). Taken together, the split-design CAR-T strategy demonstrated

sensitive antitumor activity in vivo and provided a mechanism for finely tuning the regulation of toxic side effects, underscoring its potential for clinical applications.

The split-design CAR approach improves in vivo efficacy against MM, NHL and B-ALL

We then examined the antitumor efficacy of split-design and conventional ligand-based CAR-T cells in vivo. The experimental timeline is shown in Fig. 4a. As illustrated in Figs. 4b, d, compared with the two types of conventional CAR-T cells, the sCAR-T cells exhibited superior tumor control. Notably, APRIL-redirected sCAR-T-cell therapy resulted in rapid and complete tumor clearance, with no tumor recurrence observed up to day 66. Furthermore, we noted a significant increase in the serum cytokine levels in the mice treated with sCAR-T cells compared to those in the conventional CAR-T-cell group (Fig. 4e). Throughout the experiment, the mice did not exhibit significant weight loss (Supplementary Fig. 16). In the BAFF-redirected sCAR group, one animal died on day 53, possibly caused by graft-versus-host disease (GVHD). Although there was no significant difference in the survival of the mice between the two designed BAFF-specific CAR-T-cell groups, likely due to the low affinity of BAFF for BCMA in MM, 60% of the mice in the split-design APRIL-redirected sCAR-T-cell group were still alive at 200 days, in contrast to only 20% of the mice treated with conventional APRIL CAR-T cells ($P = 0.0269$) (Fig. 4f–g). In conclusion, the split-design approach, which preserves the original properties of natural ligands, demonstrated significantly higher therapeutic efficacy in tumor control compared to conventional CAR designs.

It has been reported that every B-cell malignancy expresses at least one of the antigens, BAFFR, BCMA and TACI^{31,32}. To further validate the efficacy of BAFF-based sCAR-T cells, we extended our study to non-Hodgkin's lymphoma (NHL) models³³. As indicated in Supplementary Fig. 17a–c, conventional BAFF CAR-T cells exhibited ineffective tumor control due to their poor targeting ability, whereas BAFF-redirected sCAR-T cells effectively suppressed Raji tumor growth during drug administration in both dose groups. This finding underscores the significant improvement in treatment effectiveness achieved with the split-design approach. Serum pro-inflammatory cytokines secreted by sCAR-T cells were significantly higher than those secreted by conventional CAR-T cells (Supplementary Fig. 17d). In terms of safety, there was no significant weight loss (Supplementary Fig. 17e). Although the tumors recurred soon after drug withdrawal, the survival of the mice in the sCAR-T-cell group was significantly longer than that of the mice treated with conventional CAR-T cells (Supplementary Fig. 17f). In summary, BAFF-mediated sCAR-T cells can effectively control the growth of NHL in vivo, broaden the scope of disease treatment, and achieve significantly enhanced therapeutic effects compared to conventional BAFF CAR-T cells, once again highlighting the superiority of the split-design approach.

To assess the potential of ligand-based sCAR-T cells for treating heterogeneous B-ALL patients, we selected CD19/CD22

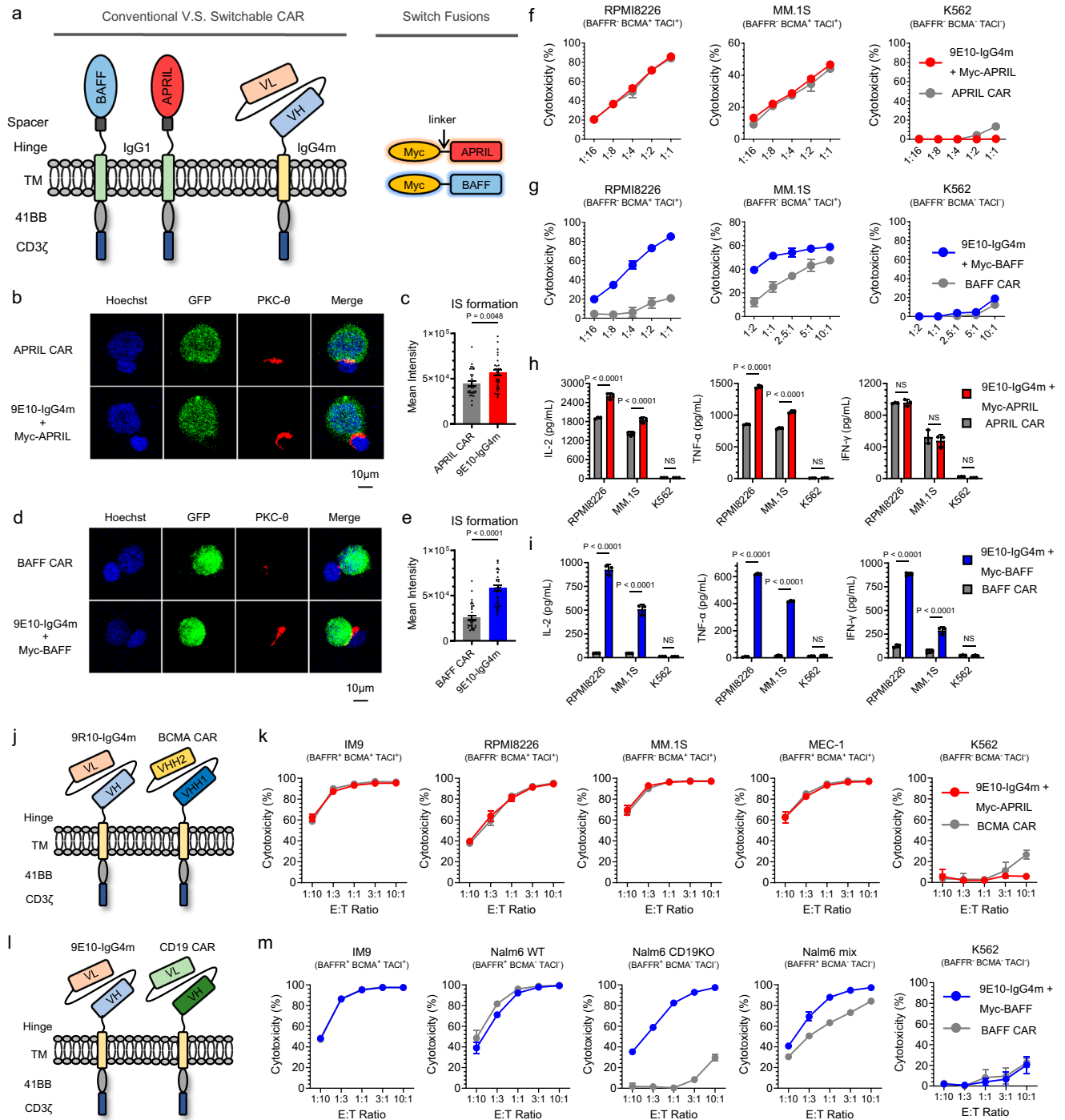
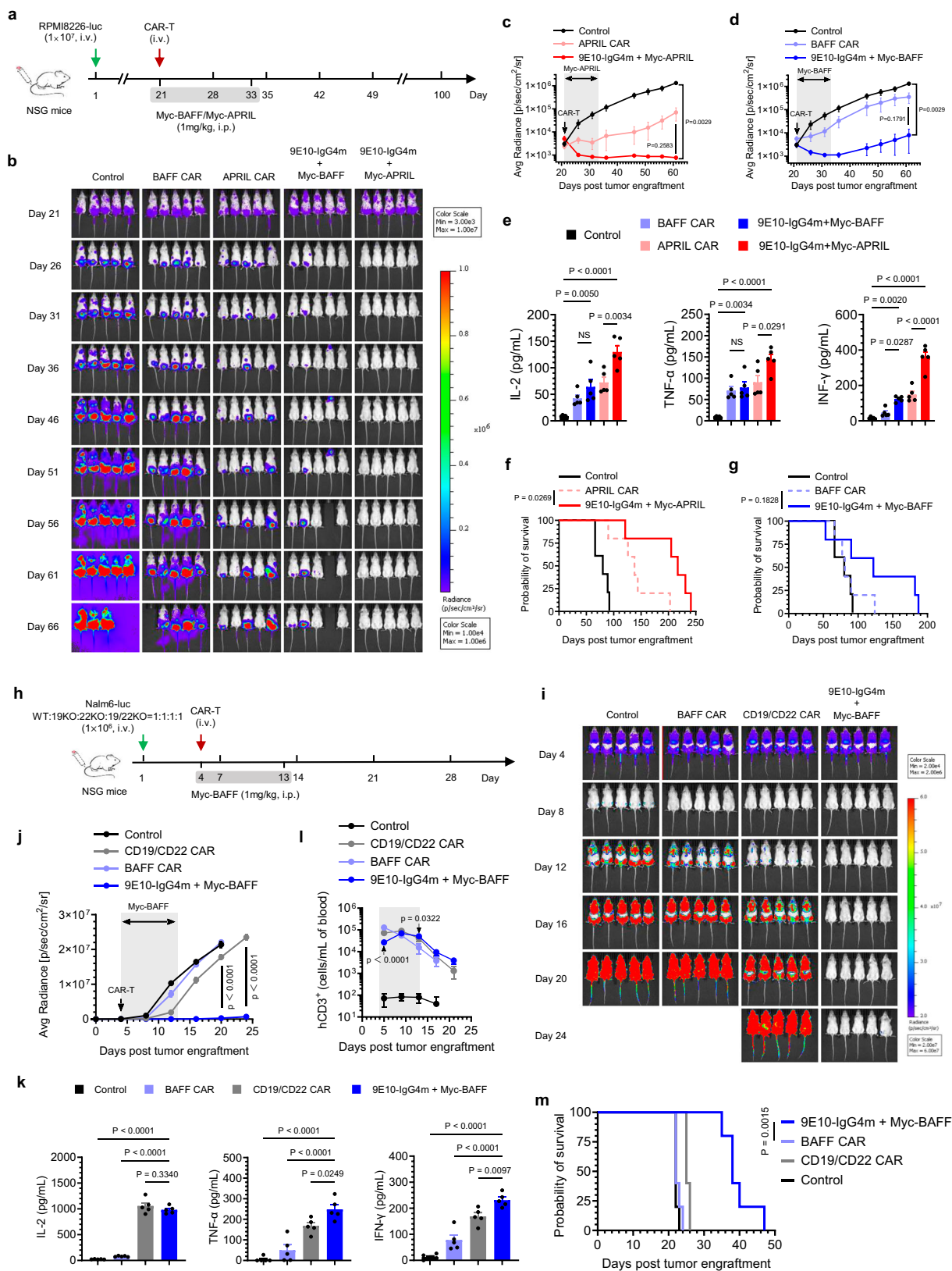


Fig. 3 | In vitro comparison of the split-design CAR approach with conventional CAR. **a** Schematic representations of ligand-based conventional and split-design CAR approaches. The extracellular domains of BAFF and APRIL were used as target moieties to generate conventional CAR-T cells, referred to as APRIL CAR and BAFF CAR, respectively. **b, d** Representative images of cell–cell conjugates captured at 100× oil objective magnification using a laser scanning confocal microscope (Nikon, A1R). APRIL or 9E10-IgG4m (pre-incubated with Myc-APRIL) CAR-T cells were co-cultured with RPMI8226-GFP cells (**b**), while BAFF or 9E10-IgG4m (pre-incubated with Myc-BAFF) CAR-T cells were co-cultured with IM9-GFP cells (**d**). Fluorescent labels included Hoechst (blue), anti- $\text{PKC-}\theta$ (red), and GFP (green) and a merged view of all stains. Scale bar = 10 μm . **c, e** Statistical analysis of the mean fluorescence intensity of $\text{PKC-}\theta$ at the IS in panels **b** and **d**, respectively. In panel **c**, sample sizes: APRIL CAR, $n = 37$; 9E10-IgG4m, $n = 39$. In panel **e**, BAFF CAR,

$n = 34$; 9E10-IgG4m, $n = 44$. All n values represent individual cells. P values were determined by paired two-tailed t -tests. **f, g** Cytotoxicity assays of conventional and split-design CAR-T cells against the indicated target cells at various E:T ratios for 24 h in triplicate. **h, i** Inflammatory cytokine release assay. Conventional CAR-T cells or sCAR-T cells along with 1 nM corresponding switches were co-cultured with the specific target cells for 24 h at an E:T ratio of 1:1 in triplicate. Two-way ANOVA multiple comparisons in Dunnett correction were used to assess significance. **j, l** Schematic representations of ligand-based split-design CAR and FDA-approved CAR, referred to as BCMA CAR (**j**) and CD19 CAR (**l**), respectively. **k, m** Cytotoxicity assays of FDA-approved CAR-T cells and split-design CAR-T cells against the indicated target cells at various E:T ratios for 24 h in triplicate. Data in this figure are representative of three independent experiments. Error bars represent mean \pm SD. NS indicates not significant. Source data are provided in the Source Data file.



CAR-T cells, which have demonstrated clinical efficacy in B-ALL patients, as controls (Supplementary Fig. 19a)^{3,34}. Having achieved similar CAR transduction efficacy (Supplementary Fig. 5b), we evaluated the cytotoxicity and cytokine production of CAR-T cells in response to different Nalm6 variants, validated by flow cytometry and western blotting (Supplementary Figs. 18a–c)³⁵. While

all CAR-T cells exhibited relevant cytotoxic effects on CD19⁺ and/or CD22⁺ Nalm6 cells, treatment with dual-antigen-knockout Nalm6 cells did not result in cross-resistance to APRIL- or BAFF-based sCAR-T cells, in contrast to the resistance that developed to CD19/CD22 CAR-T cells (Supplementary Fig. 19b). Additionally, all the CAR-T cells induced the release of cytokines in amounts

Fig. 4 | In vivo comparison of the split-design CAR approach with ligand-based conventional CARs. **a** Timeline of in vivo experiments. Consistent results were obtained in two independent experiments ($n = 5$ mice). **b** Representative bioluminescence images of mice subjected to different treatments. Colors represent the luminescence intensity (red, highest; blue, lowest). **c, d** Quantification of the average radiance (p/s/cm²/sr) of the luminescence, related to APRIL- (**c**) and BAFF- (**d**)-based CAR-T-cell therapy. Two-way ANOVA multiple comparisons in Dunnett correction were used to assess significance. **e** Evaluation of serum inflammatory cytokine release by ELISA 24 h after CAR-T-cell infusion. One-way ANOVA multiple comparisons in Tukey correction were used to assess significance. **f, g** Survival curves of the mice subjected to the indicated treatments. Survival curves were compared using the log-rank (Mantel–Cox) test. **h** Timeline of in vivo experiments. Consistent results were obtained in two independent experiments ($n = 5$ mice). **i** Representative bioluminescence images of mice subjected to different treatments. Colors represent the luminescence intensity (red, highest; blue, lowest).

j Quantification of the average radiance (p/s/cm²/sr) of the luminescence. Two-way ANOVA multiple comparisons in Dunnett correction were used to assess significance, comparing 9E10-IgG4m CAR-T (with Myc-BAFF) and CD19/CD22 CAR-T. **k** Evaluation of serum inflammatory cytokine release by ELISA 24 h after CAR-T-cell infusion. One-way ANOVA multiple comparisons in Dunnett correction were used to assess significance. **l** Assessment of the presence of persistent human CD3⁺ (hCD3⁺) T cells in peripheral blood by flow cytometry over a 3-week follow-up period. Two-way ANOVA multiple comparisons in Dunnett correction were used to assess significance, comparing 9E10-IgG4m CAR-T (with Myc-BAFF) with BAFF-CAR-T at each time point. **m** Survival curves of mice subjected to the indicated treatments, compared using the log-rank (Mantel–Cox) test. All n represents biological replicates from different mice. Data in this figure are representative of one of two independent experiments. Error bars represent mean \pm SEM. NS indicates not significant. Source data are provided in the Source Data file.

correlated with the degree of cytotoxicity (Supplementary Fig. 19c).

To further explore the therapeutic potential of BAFF-redirection sCAR-T cells in heterogeneous leukemia with antigen escape variants, we established a xenograft model of B-ALL using the four types of Nalm6 variants mentioned above (Fig. 4h). As illustrated in Fig. 4i–j, BAFF-based sCAR-T cells exhibited significantly superior disease control in heterogeneous leukemia compared to conventional BAFF CAR-T cells. Notably, CD19/CD22 CAR-T cells allowed rapid tumor recurrence in mice due to their inability to target CD19/CD22 antigen escape variants. Following CAR-T-cell infusion, the pro-inflammatory cytokine levels induced by BAFF-redirection sCAR-T cells were significantly higher than those in the other groups (Fig. 4k). Twenty-four hours after CAR-T-cell infusion (Fig. 4l), significantly decreased numbers of BAFF-redirection sCAR-T cells were detected because sCAR-T cells were recruited to the early tumor focus¹⁸. However, upon the elimination of tumor cells, sCAR-T cells underwent significant expansion in response to antigen stimulation, resulting in large numbers of circulating T cells in the peripheral blood. Throughout the treatment period, no significant weight loss was observed in the mice (Supplementary Fig. 20). Survival was significantly prolonged following sCAR-T-cell treatment compared to all other treatments (Fig. 4m). Collectively, our findings highlight the superior therapeutic efficacy of the split-design BAFF-based CAR-T-cell approach over the conventional strategy, especially in terms of its potential applications in overcoming tumor heterogeneity and antigen loss.

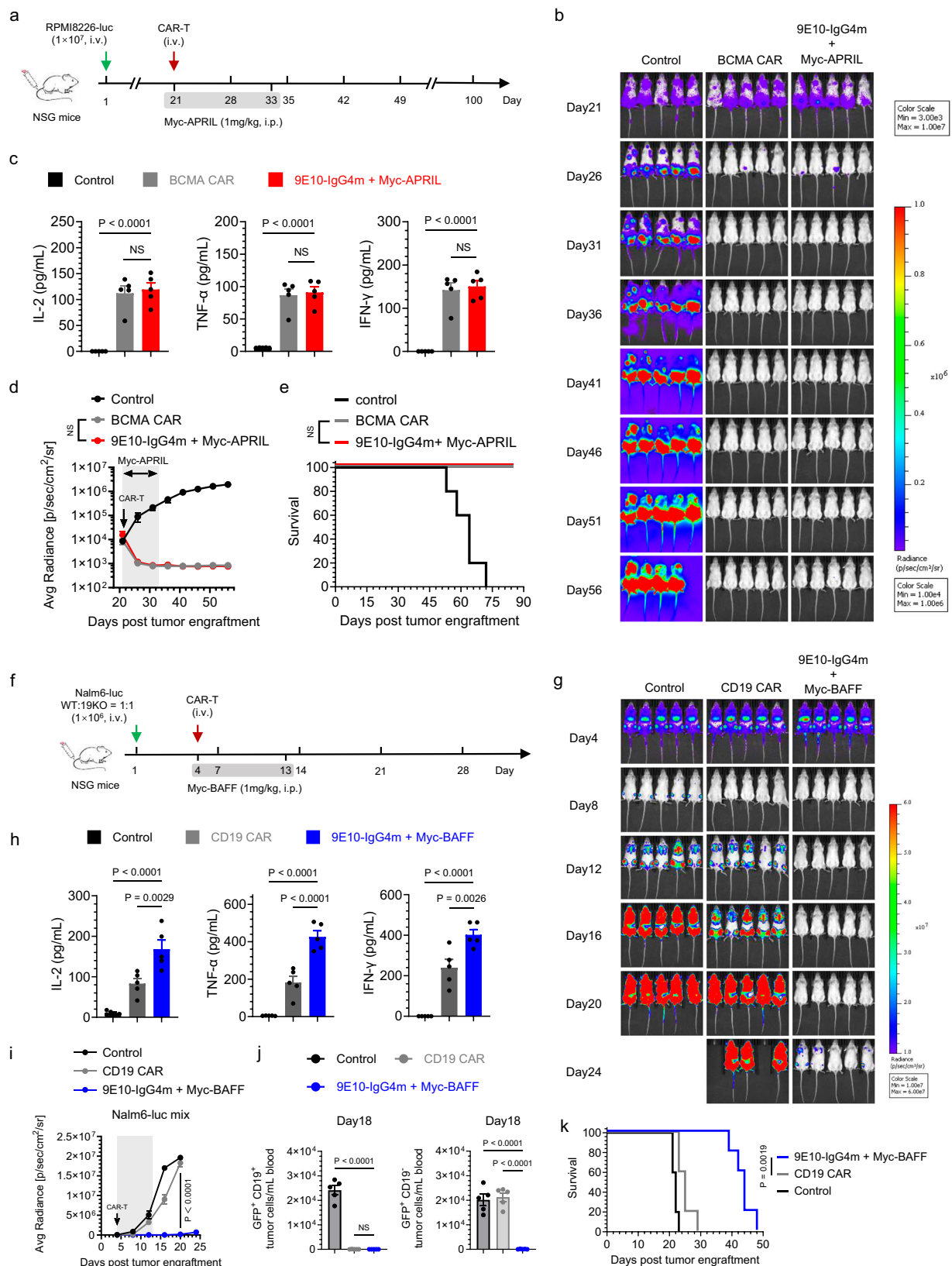
Clinical translational potential of the split-design ligand-based CAR-T system

To evaluate the clinical application potential of the split-design ligand-based CAR-T cells, we compared their efficacy against FDA-approved CAR-T-cell therapies, specifically CD19 CAR-T cells (Tisa-cel) and BCMA CAR-T cells (Cilta-cel). Consistent with our in vitro findings, APRIL-redirection sCAR-T showed comparable tumor clearance rates and serum cytokine release to those of BCMA CAR-T cells (Figs. 5a–d). No significant weight loss was observed in mice during treatment (Supplementary Fig. 21), and all the mice in both treatment groups survived without disease recurrence at the end of the experiment (Fig. 5e), highlighting the use of split-design APRIL-based CAR-T cells as a promising strategy for MM treatment. Given that BAFF-redirection sCAR-T cells were less effective than CD19 CAR-T cells in vitro, we evaluated the potential advantages of BAFF-redirection sCAR-T cells in overcoming CD19 antigen escape in vivo. In the B-ALL immune escape model established with Nalm6-WT and Nalm6-19KO cells, BAFF-based sCAR-T cells demonstrated superior tumor clearance, increased cytokine release, improved persistence, and significantly prolonged survival in scenarios involving CD19 antigen escape (Figs. 5f–i, 5k, Supplementary Figs. 22a, b). By day 18 of the experiment, only CD19-negative tumor cells were detected in the peripheral blood of the CD19

CAR-T-treated mice, but no tumor cells were detectable in the sCAR-T-treated mice (Fig. 5j, Supplementary Fig. 22c). Notably, while tumor relapse was observed on day 36 after BAFF-based sCAR-T-cell treatment, we did not detect surface BAFFR loss on leukemic cells, suggesting that recurrence was likely associated with discontinuation of switch administration but not antigen escape (Supplementary Fig. 22d). In the B-NHL immune escape model, in which Raji-WT and Raji-19KO cells were s.c. transplanted into mice (Supplementary Fig. 23a–b), the results were consistent with those observed in the leukemia model (Supplementary Fig. 23c–f), underscoring the advantage of BAFF-redirection sCAR-T cells in overcoming antigen escape after CD19 CAR-T-cell therapy. These results further confirm that the split-design ligand-based CAR-T-cell system exhibits multitargeting capabilities, broad-spectrum efficacy, and clinically relevant compared to FDA-approved CAR-T-cell therapies.

In vivo synergistic effects of the split-design ligand-based CAR-T-cell system

Combining antigen-specific approaches to achieve precise tumor identification can significantly enhance therapeutic outcomes^{36–38}. Directing a single CAR-T-cell toward distinct antigens offers an alternative to broad-spectrum therapy. However, the conventional method of designing two separate batches of CAR-T cells with different antigen specificities is prohibitively costly. Hence, a drug-gated sCAR system in which different drugs are introduced to activate CARs targeting various antigens could prove invaluable^{39,40}. To demonstrate the feasibility of using a split-design CAR as a switchboard (Fig. 6a), we first established an orthotopic RPMI8226 (BCMA⁺ TACI⁺ MM) model. After tumor clearance was achieved with Myc-APRIL, the mice were rechallenged with Nalm6 (BAFFR⁺ B-ALL) tumor cells and treated with the alternative switch, Myc-BAFF (Fig. 6b). As shown in Fig. 6c–d, both tumor burdens were effectively managed by utilizing different switches with a single CAR, whereas tumor recurrence occurred in the mice treated with conventional CAR-T cells combination. The percentage survival on day 75 was 100% for the sCAR-T-cell therapy group and 0% for the conventional CAR-T-cell therapy group ($P < 0.0001$) (Fig. 6e). Consistent with previous results, mice with MM single tumors treated with Myc-APRIL exhibited rapid tumor clearance and significantly prolonged survival (Supplementary Figs. 24a, b). Twenty-four hours after the first dose of Myc-APRIL and Myc-BAFF, the serum of mice in the sCAR-T-cell group exhibited significantly higher levels of proinflammatory cytokines than those in the conventional CAR-T-cell group (Fig. 6f, Supplementary Fig. 24c). At the endpoint of the switch treatment (day 18), we detected a substantial number of sCAR-T cells in the peripheral blood of mice, which was significantly higher than the number of conventional CAR-T cells in the conventional CAR-T-cell group (Fig. 6g, Supplementary Fig. 24d). As expected, in the absence of Myc-BAFF, sCAR-T cells failed to control the second tumor, Nalm6,



and induce cytokine production and T-cell expansion, suggesting the absence of cross-inhibitory effects between each switch and highlighting the necessity of alternative dosing regimens to control B-cell malignancies via antigen switching. While the mice in the sCAR-T-cell group exhibited slight weight loss during Myc-BAFF administration, they eventually regained normal weight after treatment was

completed (Supplementary Fig. 25a-b). In summary, compared with conventional CAR-T-cell therapy, the split-design CAR-T-cell system enables the use of different switches as regulators to sequentially modulate T-cell functions, allowing the sequential targeting of different tumor types and driving synergistic *in vivo* activities to further reduce tumor burden, with significantly improved results.

Fig. 5 | In vivo comparison of the split-design CAR approach with the FDA-approved CARs. **a** Timeline of in vivo experiments. Consistent results were obtained in two independent experiments ($n = 5$ mice). **b** Representative bioluminescence images of mice subjected to different treatments. Colors represent the luminescence intensity (red, highest; blue, lowest). **c** Evaluation of serum inflammatory cytokine release by ELISA 24 h after CAR-T-cell infusion. One-way ANOVA multiple comparisons in Dunnett correction were used to assess significance. **d** Quantification of the average radiance ($p/s/cm^2/sr$) of the luminescence. Two-way ANOVA multiple comparisons in Sidak correction were used to assess significance, comparing 9E10-IgG4m CAR-T (with Myc-APRIL) with BCMA CAR-T. **e** Survival curves of mice subjected to the indicated treatments, compared using the log-rank (Mantel–Cox) test. **f** Timeline of the in vivo experiments. Consistent results were obtained in two independent experiments ($n = 5$ mice). **g** Representative bioluminescence images of mice subjected to different treatments. Colors represent the

luminescence intensity (red, highest; blue, lowest). **h** Evaluation of serum inflammatory cytokine release by ELISA 24 hours after CAR-T-cell infusion. One-way ANOVA multiple comparisons in Dunnett correction were used to assess significance. **i** Quantification of the average radiance ($p/s/cm^2/sr$) of the luminescence. Two-way ANOVA multiple comparisons in Dunnett correction were used to assess significance, comparing 9E10-IgG4m CAR-T (with Myc-BAFF) with CD19 CAR-T. **j** Assessment of the presence of tumor cells (GFP⁺ CD19⁺ or GFP⁺ CD19⁻) in peripheral blood by flow cytometry on the 18th day of the experiment. One-way ANOVA multiple comparisons in Dunnett correction were used to assess significance. **k** Survival curves of the mice subjected to the indicated treatments, compared using the log-rank (Mantel–Cox) test. All n represents biological replicates with different mice. Data are in this figure representative of one of two independent experiments. Error bars represent mean \pm SEM. NS indicates not significant. Source data are provided in the Source Data file.

Discussion

The development of CAR-T-cell therapy has had a significant impact on the field of cancer immunotherapy; however, it is concerning that relapse rates can reach 40–60% in patients with B-cell malignancies^{41–44}. To address these concerns, compensatory strategies mediated by antibody combinations or multispecific ligands have been explored successfully in several clinical trials^{3,4,45,46}. While these studies have demonstrated the feasibility of co-targeting different neoantigens to prevent antigen escape, these systems generally do not allow optimal CAR structure design or facile modulation of CAR-T-cell activity. Importantly, this is a systematic comprehensive investigation into the importance of ligand-mediated CAR-T cells in a split design to achieve improved efficacy over conventional CAR approaches.

While scFv-based CAR-T cells have shown great success in the clinic, they also present problems related to stability, immunogenicity, and antigen escape, which pose challenges for the further translation of some CAR-T-cell therapies^{47,48}. As an alternative approach, ligand-based CAR designs have proven to be advantageous in some circumstances compared to scFv-based designs, and several translational aspects are undergoing clinical testing^{12,15,49–51}. A phase I clinical trial (NCT05312801) involving BAFF CAR-T cells (LMY-920) is underway, and the results are pending. Furthermore, both APRIL and BAFF have been explored as targeting moieties for toxin delivery against various B-cell malignancies^{26,52–55}. However, a phase I/II clinical trial (NCT03287804) of BCMA/TACI bispecific CAR-T cells (AUTO2), which utilize truncated APRIL as the antigen-binding domain, to treat patients with relapsed/refractory MM was terminated early due to poor efficacy. While the APRIL CAR was well tolerated, responses were observed in 45.5% of patients^{56,57}. Compared with those of the BCMA CARs (Ide-cel and Cilta-cel), the APRIL CAR showed weaker T-cell activation, cytotoxicity and soluble antigen binding *in vitro*⁵⁷. These deficiencies were likely due to the use of APRIL as an antigen recognition domain. As members of the TNF family, APRIL and BAFF must assemble as homotrimers to promote optimal binding to receptors. To achieve greater efficacy, trimeric APRIL- and BAFF-based CARs have been developed by connecting three ligand monomers via linkers^{13,14}. However, conventional structures based on TNF ligands, particularly BAFF, have limitations due to their type II transmembrane protein structure. In contrast to CARs, which are type I transmembrane proteins whose N-terminus lies in the distal membrane, the inherent conformation of ligands is inverted for use as the extracellular region of a CAR construct. This not only compromises ligand efficiency but also carries the risk of adverse effects since the C-terminus of these ligands is important for receptor recognition. These findings suggested that T cells expressing APRIL do not bind to the target satisfactorily, which directly contributes to the limited ability of the APRIL CAR to achieve clinical remission in clinical trials. Therefore, we suspect that the use of BAFF to construct CAR-T cells may also have certain limitations. In this context, we explored a split CAR design to harness the multispecificity of ligands. Surprisingly, conventional BAFF

CAR exhibited markedly reduced efficacy, particularly against BAFF single-positive ALL cell lines, which may be due to the strong trimeric dependence of BAFFR receptor binding to BAFF ligands. Furthermore, the preparation process did not utilize the transposon system, which may also contribute to the inferior efficacy of the BAFF CAR. Both APRIL- and BAFF-based switches retained homotrimer structures, and the flexibility of Myc tag fusion site selection guaranteed optimal CAR-T-cell-redirected activities against various tumor cells.

Efforts to optimize the simultaneous design of sCAR hinges and switch labeling sites are crucial for enabling efficient IS formation and optimal sCAR-T-cell activity. Consequently, we refined the optimal ligand-based sCAR design by fusing the Myc tag to the N-terminus of ligand ectodomains. These fusions paired with sCAR-T cells with a shortened 12-aa IgG4m hinge, facilitating the efficient formation of synapses^{18,58,59}. Among all the candidates, the optimized sCAR-T-cell construct significantly improved the geometric arrangement of IS between cancer cells and T cells, leading to efficient tumor clearance and cytokine production in response to multiple cell lines and patient samples. Importantly, our structurally optimized sCAR-T cells exhibited desirable breadth and potency *in vitro* and *in vivo* against various B-cell malignancies, overcoming the limited antitumor activity associated with conventional ligand-based CAR-T-cell therapy. This highlights the promising advantages of split CAR design, particularly when natural ligands or receptors are utilized as targeting moieties, to meet functional requirements effectively.

We comprehensively evaluated the relative cytotoxicity of BAFF/APRIL-based sCAR-T cells in comparison to Tisa-cel (CD19 CAR-T) and Cilta-cel (BCMA CAR-T) across a range of cell lines *in vitro*, as well as in various xenograft models *in vivo*. BAFF-based sCAR-T cells demonstrated distinct advantages over Tisa-cel, particularly in scenarios where CD19 antigens had escaped; however, their cytotoxicity against single and double positive cell lines was slightly lower than that of CD19 CAR-T cells. This difference may be attributed to significantly lower target densities of BAFFR/BCMA/TACI compared to CD19 antigens. Conversely, the overall activity of APRIL-based sCAR-T cells remained comparable to that of Cilta-cel, with reduced efficacy noted exclusively in cell lines expressing BCMA antigens at very low densities. This reduction may be related to Cilta-cel's dual BCMA-targeting VHs, which recognize two different epitopes of the BCMA antigens. These results are promising, though certain aspects fall short when compared to the performance of FDA-approved CAR-T therapies. Nevertheless, the split design CAR approach offers a broader range of indications, multi-target combinations, and flexibility for modifications, highlighting its significant potential for clinical translation.

The primary objective of the sCAR-T-cell strategy is to enhance the versatility for controlling tumor variants by targeting different antigens with a single CAR⁶⁰. Therefore, we characterized this approach in various preclinical animal models with clinical relevance. We modeled CD19 and CD22 antigen loss by gene knockout in B-ALL Nalm6 cell lines and observed continued susceptibility to tumor

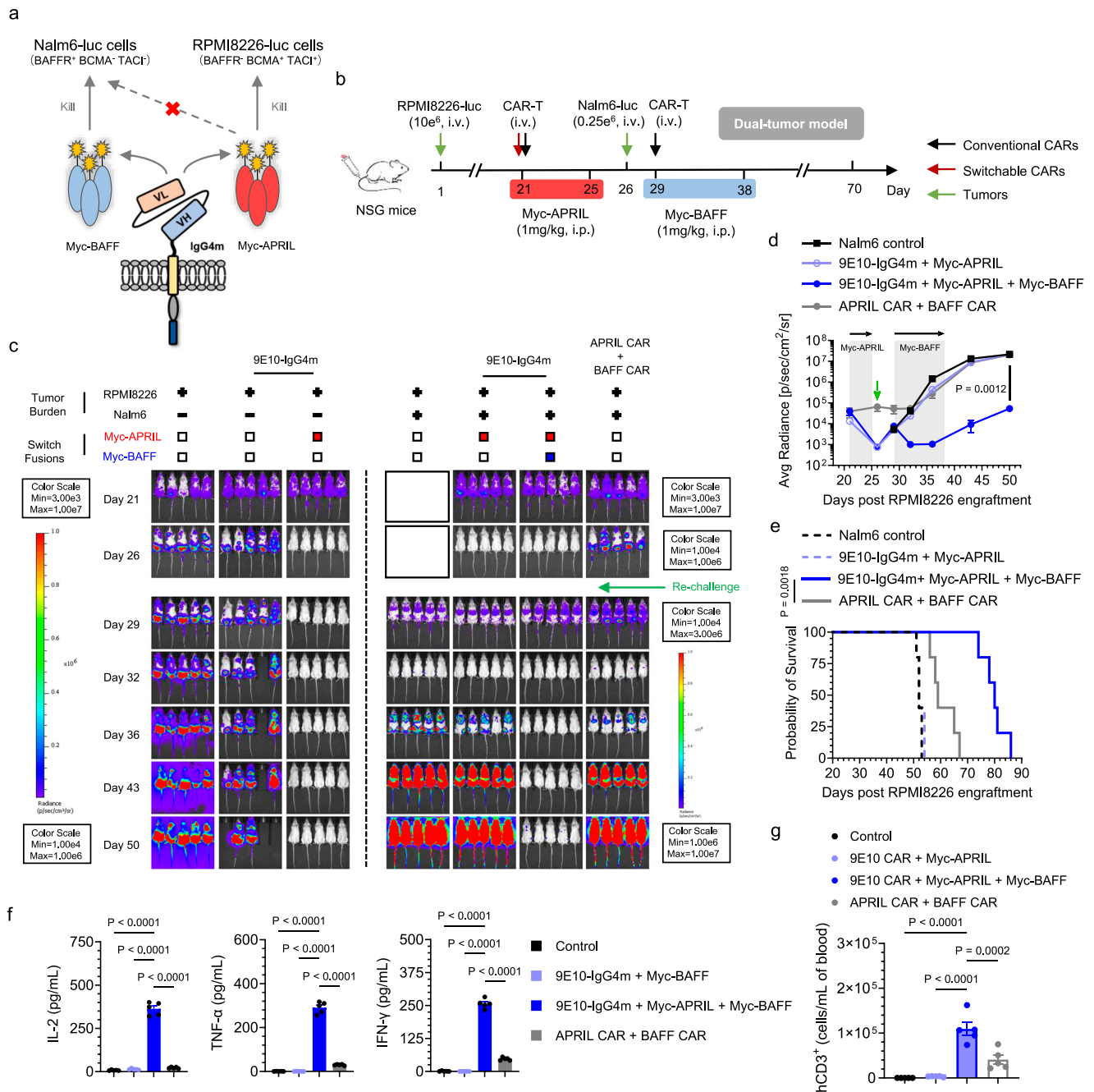


Fig. 6 | In vivo synergies of the split-design ligand-based CAR-T-cell system.

a Schematic representation of the design utilizing various switches to redirect sCAR-T cells to specific tumors. **b** Timeline of the in vivo model illustrating the synergistic efficacy of sequential tumor control in MM using Myc-APRIL and B-ALL using Myc-BAFF. Twenty-one days after RPMI8226 tumor engraftment, mice were i.v. administered 15×10^6 corresponding CAR-T cells. Myc-APRIL was i.p. administered daily for 5 days to manage RPMI8226 tumor cells. Following this, Nalm6 cells (0.25×10^6 cells) were i.v. injected 6 days later, and sCAR-T cells were redirected to control B-ALL tumors through daily i.p. administration of Myc-BAFF for 10 days. Conventional APRIL and BAFF CAR-T cells were injected on days 21 and 29, respectively. Consistent results were obtained in two independent experiments ($n = 5$ mice). **c** Representative bioluminescence images of mice under different treatment conditions. Colors indicate the luminescence intensity (red, highest; blue, lowest). **d** Tumor burden of the MM and B-ALL dual-tumor model over time following Nalm6 rechallenge, quantified as the average radiance (p/s/cm²/sr)

the luminescence. Two-way ANOVA multiple comparisons in Tukey correction were used to assess significance, comparing 9E10-IgG4m CAR-T in combination with Myc-APRIL and Myc-BAFF versus the combination of the APRIL CAR-T and BAFF CAR-T. **e** Survival curves depicting the outcomes of the mice subjected to the indicated treatments, compared using the log-rank (Mantel-Cox) test. **f** Serum inflammatory cytokine release was evaluated by ELISA 24 h after the first dose of Myc-BAFF. One-way ANOVA multiple comparisons in Dunnett correction were used to assess significance. **g** On the 39th day of the experiment, the presence of persistent human CD3⁺ (hCD3⁺) engineered CAR-T cells in the peripheral blood was assessed in Nalm6-rechallenged mice by flow cytometry. One-way ANOVA multiple comparisons in Dunnett correction were used to assess significance. All n represents biological replicates with different mice. Data in this figure are representative of one of two independent experiments. Error bars represent mean \pm SEM. Source data are provided in the Source Data file.

eradication in vivo by BAFF-based sCAR-T cells but not CD19/CD22 CAR-T cells. Clinically, resistant disease is characterized by tumor variants that progress following treatment initiation. A split-design CAR strategy using APRIL- and BAFF-based switches could serve as an ideal single infusion therapy for various B-cell malignancies. To that end, we further evaluated the in vivo efficacy of sCAR-T cells with different switches against sequential challenges with different tumors, including MM and B-ALL cells. The modular design of our ligand-based sCAR platform allowed convenient redirection and adjustment of the target specificity using a universal CAR harboring multiple switches. Through a split-design CAR strategy, we can leverage a single lentiviral structure to create uniform CAR-T-cell products addressing various antigen attributes. These features are highly desirable for minimizing the risk of developing escape variants and simplifying the clinical implementation of CAR-T-cell therapy.

While some of our split designs of ligand-based sCARs have already demonstrated in vitro and in vivo efficacy, others still require further optimization. For example, we did not include scFv-based adapter CARs in the comparison range of the study. Since our initial intention was to generate ligand-based multitarget CAR-T cells, the present study aimed to demonstrate the importance of a split design and proper configuration for ligand-based CAR-T cells. In addition, the safety data of the split-design ligand-based approach are insufficient, and more exploration is still needed in the future. Finally, the relative activities of the sCAR and regular CAR have been validated only on a second-generation CAR backbone (lentiviral vector), which may greatly reduce CAR activity^{56,57}, especially that of BAFF CAR.

In conclusion, we developed an optimized split-design CAR-T-cell strategy based on APRIL and BAFF ligands that faithfully replicates the natural ligand structure and targeting specificity, offering distinct advantages over the conventional CAR-T-cell approach, including optimal IS formation and enhanced antitumor efficacy (Supplementary Fig. 27). Notably, synergistic ligand-based sCAR-T-cell therapy represents a significant advance over current CAR-T-cell approaches, as it addresses clinical challenges such as immune escape while providing high antitumor potency and persistence against antigenically heterogeneous tumors. Therefore, our sCAR-T-cell strategy is promising as a therapeutic option for treating various B-cell malignancies characterized by heterogeneous antigen expression in clinical settings.

Methods

Study approval

All experiments involving human materials were approved by the Clinical Research Ethics Committee of the Huazhong University of Science and Technology Union Shenzhen Hospital. Healthy volunteers provided informed written consent prior to participation.

Animal experiments were approved by the Animal Care and Use Committee of Peking University Shenzhen Graduate School and were conducted in accordance with the national and international guidelines for the ethical treatment of animals.

Experimental design

The aim of this study was to develop optimal, multitargeted, and regulatable CAR-T cells. We harnessed the multitargeting properties of the natural ligands APRIL and BAFF to broadly target most B-cell malignancies. Currently, conventional APRIL- or BAFF-based CAR-T cells may not reliably maintain the trimer conformation, which can lead to nonspecific toxicity or reduced antitumor activity. Our hypothesis was that by constructing the extracellular domains of APRIL and BAFF separately from CAR-T cells, we could ensure the correct conformation of ligand proteins, optimal binding to receptors, and enhanced antitumor activity. The efficacy of split-design ligand-based CAR-T cells was evaluated through in vitro immune synapse formation, cytotoxicity, and cytokine release assays, as well as through xenograft efficacy studies. In vitro, experiments were conducted in

triplicate, while the sample sizes for in vivo studies were determined empirically to ensure sufficient statistical power following established standards for the techniques utilized in the study. Mice were randomly assigned to treatment groups to avoid statistically significant differences in the baseline tumor burden. Data analysis was not performed in a blinded manner.

Cell lines and culture conditions

All human malignant hematologic cell lines, including Nalm6, IM9, Raji, RPMI8226, MM.1S, K562, were directly obtained from the American Type Culture Collection (ATCC). These cell lines were cultured in complete RPMI-1640 media (HyClone, SH30255.01), supplemented with 10% heat-inactivated FBS (Yoshi, A1015), 1% penicillin–streptomycin (P/S), 0.1 mM non-essential amino acids (NEAA), 6 mM L-glutamine (L-Glu) and 1 mM sodium pyruvate (SP). HEK293T cells were purchased from Thermo Fisher Scientific and maintained in high-glucose complete DMEM (Gibco, C11995500BT) supplemented with 10% FBS, 1% P/S, 0.1 mM NEAA, 6 mM L-Glu and 1 mM SP. The FreeStyle 293 suspension cell line was obtained from Sino Biological, Inc., and cultured in SMM293-TII media (Sino Biological, M293TII-N).

Structure designs of CARs and switch fusions

All CAR structures comprised the following elements in a sequential arrangement: the EF1 α promoter, the CD8 signaling sequence, the antigen binding domain, the transmembrane domain, the 4-1BB costimulatory domain, and the CD3 ζ signal transduction domain. A schematic diagram of the component connections for each CAR is provided in Supplementary Fig. 5a. The antigen-binding domain for all three 9E10-based CARs was the anti-Myc scFv derived from clone 9E10. Specifically, the 9E10-CD8 CAR features a CD8 hinge region and transmembrane domain, the 9E10-CD28 CAR contains a CD28 hinge region and transmembrane domain, and the 9E10-IgG4m CAR contains an IgG4m hinge region and a CD8 transmembrane domain. Additionally, conventional APRIL- or BAFF-based CARs employ the extracellular domain of APRIL or BAFF as their antigen-binding domain, which features a Myc tag at the N-terminus. Both constructs included the IgG1 hinge region and the CD28 transmembrane domain, with a short spacer interval inserted between the hinge region and the ligand, following the methods of Wong and Lee^{12,15}. For CD19 CAR-T cells, the scFv clone FMC63 targeted CD19, which was structured as shown in the Figure and was consistent with tisagenlecleucel (Tisa-cel). For the BCMA CAR-T cells, two VHH domains targeted different epitopes of BCMA, which was structured as shown in the Figure and was consistent with ciltacabtagene autoleucel (Cilta-cel). For the CD19/CD22 bispecific CAR, the CD19-targeting scFv (clone FMC63) and CD22-targeting scFv (clone M971) were utilized, and M971 was connected between the VL and VH of the FMC63 scFv using flexible GGGGS linkers to create a loop structure.

The gene sequences of the natural ligands APRIL (TNFSF13, O75888) and BAFF (TNFSF13B, Q9Y275) were obtained from UniProt.org. GenScript Biotech, Inc., synthesized the genes, which were subsequently inserted into the pCAGGS expression vector. Truncated APRIL ligand (116-250aa) and truncated BAFF ligand (134-285aa) were used for switch construction. A flexible GGGGS linker was chosen to attach the Myc tag to either the N- or C-terminus of APRIL and BAFF ligands. Additionally, a 6 \times His tag was incorporated as a purification marker and separated by a thrombin cleavage site.

Expression and purification of switch fusions

Switch fusions were transiently expressed using the FreeStyle HEK293 expression system. Briefly, transfection was initiated when the cell density of FreeStyle 293 suspension cells reached 3×10^6 /mL. Subsequently, 100 μ g of the expression vector plasmid was diluted in Opti-MEM (Gibco, 31985-070) and mixed with Opti-MEM containing 125 μ g

of PEI MAX MW40000 (Polysciences, Inc., 24765-1). After a 30-minute incubation, the mixture was added to the cell suspension. The cells were then agitated at 125 rpm in a 5% CO₂ environment at 37 °C. The expression cultures were harvested 72–96 h post-transfection by centrifugation at 350 × *g* and subjected to purification using Ni Sepharose 6FF (Solarbio, P2010). The bound protein was eluted using an elution buffer composed of 150 mM imidazole, 300 mM NaCl, and 50 mM sodium phosphate at pH 7.4. The desired fractions were combined and dialyzed against PBS overnight. After 16 h of digestion with thrombin at room temperature, the 6×His tag was removed. Finally, the 6×His tag and multimeric impurities were eliminated via size exclusion chromatography utilizing the ÄKTA pure™ chromatography system (GE Healthcare) equipped with HiLoad 16/600 Superdex 200 pg (GE Healthcare, 28989335). The identity and purity of the switches were confirmed through SDS-PAGE analysis. The purified switches were then aliquoted and stored frozen for long-term preservation.

Molecular conformation analysis by SEC

The native-state molecular polymer conformation of the switches was assessed using SEC. The purified proteins were first filtered through a 0.2 μm filter (Millex-GV, SLGVR33RB), then loaded onto a Superdex 200 Increase 10/300GL column (Cytiva, 28990944), and separated using an AKTA pure system operating at a flow rate of 0.25 ml/min at room temperature. To calibrate the purification system, a protein mixture comprising bovine serum albumin (ExCell Bio, C-BSA00100), ovalbumin (Shanghai yuanye Bio-Technology, S12015), carbonic anhydrase (Shanghai yuanye Bio-Technology, S10157), ribonuclease A (Shanghai yuanye Bio-Technology, R21097), and aprotinin (Shanghai yuanye Bio-Technology, S10089) was utilized as a standard. The retention volume of each elution peak was determined through integration using UNICORN 6.3 software.

Isolation of peripheral blood mononuclear cells (PBMCs)

Anonymized healthy donor blood was provided by the Department of Hematology, Huazhong University of Science and Technology Union Shenzhen Hospital. PBMCs utilized for CAR-T-cell preparation were isolated from blood using density gradient centrifugation (1000 × *g*, 30 min at room temperature without break) with Ficoll-Paque PLUS (Cytiva, 17144003). Human PBMCs were isolated from the interphase and washed several times with DPBS. Subsequently, the isolated PBMCs were cryopreserved at a concentration of 10 × 10⁸/mL in a solution containing 10% DMSO in FBS.

CAR-encoding lentivirus production

To generate lentivirus, 1.5 × 10⁶ 293 T cells were seeded in 6-well plates 24 h prior to transfection. When the cell density reached 80%–90%, Lipofectamine 2000 (Invitrogen, 11668-019) was used to transfect each well with 0.75 μg of VSVG envelope plasmid, 1.8 μg of pMDL packaging plasmid, 1.8 μg of pRSV-Rev packaging plasmid, and 2.25 μg of CAR plasmid, all of which were mixed in OPTI-MEM. The medium was replaced with fresh media 6 h later, and the lentiviral supernatant was collected at 48 h post-transfection. The viral supernatant was aliquoted and stored at –80 °C for future use.

Transduction and culture of CAR-T cells

The isolated T cells were thawed and activated with DynaBeads Human T-Activator CD3/CD28 (Gibco, 11141D) for 48 hours in X-VIVO 15 medium (LONZA, 04-418Q) supplemented with 5% FBS and 300 IU/mL IL-2 (GenScript, Z00368-50). Subsequently, the cells were infected with lentivirus using a centrifugation protocol (1000 × *g*, 30 min, 25 °C). CAR-T cells were expanded in X-VIVO¹⁵ medium (5% FBS) supplemented with 10 ng/mL IL-7 (GenScript, Z02704) and 5 ng/mL IL-15 (GenScript, Z03308). CAR-T cells were expanded to 10 days post-activation for subsequent experiments.

B-cell malignancy patients and clinical data

Peripheral blood or bone marrow samples were collected from patients diagnosed with B-cell malignancies after providing informed consent. Patient samples were provided by the Department of Hematology, Huazhong University of Science and Technology Union Shenzhen Hospital. Peripheral blood mononuclear cells (PBMCs) were isolated from these patient samples using established protocols, and the selection of samples was guided to study reports. Clinical and laboratory data were extracted from electronic medical records. Informed consent has been obtained from all study participants for the publication of clinical information.

Generation of CD19- or/and CD22-knockout cell lines

We employed CRISPR/Cas9 gene editing techniques to generate CD19- or/and CD22-knockout Nalm6-GL cell lines. Lenti-CRISPR plasmids were designed to deliver Cas9 along with specific guide RNA (gRNA) sequences targeting the CD19 antigen (AAGCGGGACTCCCGAGACC on exon 3) or the CD22 antigen (GGATCATCAGAAGACCCCCC on exon 6). The construction process followed established protocols. Monoclonal cell lines were sorted and screened to ensure purity and consistent antigen density. To confirm genotypic alterations, all KO cell lines underwent assessment for CD19 and CD22 surface expression using flow cytometry and western blotting. For western blot, anti-human CD19 antibody (Boster, BM4935) and anti-human CD22 antibody (Boster, BM4178) were used to verify the KO efficiency³⁵.

Generation of K562 cell variants with gradient expression of BCMA

Genes encoding the full-length BCMA antigen were synthesized by GenScript and cloned into the pLV lentiviral plasmid. To prepare lentivirus, 1.5 × 10⁶ 293 T cells were seeded in 6-well plates 24 h prior to transfection. Lipofectamine 2000 (Thermo Fisher Scientific, 11668019) was used to co-transfect third-generation lentiviral packaging plasmids (pMDL, pRSV-REV, and pVSV-G) with the pLV plasmid into 293 T cells, following the manufacturer's instructions for lentivirus preparation. After 48 h, the virus-containing medium was collected. The lentiviral supernatant was used to transduce the wild-type K562 cell line, and monoclonal clones with varying densities of BCMA antigen were sorted using flow cytometry.

Flow cytometry analysis

The following antibodies were used for staining: APC anti-human BAFFR (BioLegend, 316916), PE anti-human BCMA (BioLegend, 357504), PE anti-human TACI (BioLegend, 311906), APC anti-human CD3 (BioLegend, 300312), Pacific Blue anti-human CD3 (BioLegend, 300329), FITC anti-human CD45 (BioLegend, 304038), PE anti-human CD22 (BioLegend, 302506), APC anti-human CD19 (BioLegend, 302212), Alexa Fluor 647 goat anti-mouse IgG (H+L) (Invitrogen, A21235), Alexa Fluor 647 F(ab')₂ fragment of goat anti-mouse IgG (Invitrogen, A21237), and FITC goat pAb to Myc tag (Abcam, ab1263). These antibodies were diluted to a concentration of 1 μg/ml for staining the cell samples in PBS. The transduction efficiency of 9E10-based CAR-T cells and CD19/CD22 bispecific CAR-T cells was assessed by staining with anti-mouse IgG (H+L) F(ab')₂ fragment-Alexa Fluor 647. The transduction efficiency of APRIL- and BAFF-based conventional CAR-T cells was determined using FITC anti-Myc tag staining. The surface expression of BAFFR, BCMA and TACI antigens on multiple B-cell malignant cell lines or primary patient samples was analyzed using APC-conjugated anti-human BAFFR, PE-conjugated anti-human BCMA and PE-conjugated anti-human TACI. For T cells in *in vivo* assays, samples were stained with FITC-conjugated anti-human CD45 and APC-conjugated anti-human CD3. Tumor cells *in vivo* were identified as GFP⁺ and further analyzed using APC-conjugated anti-human BAFFR or APC-conjugated anti-human CD19 antibodies. To exclude dead cells from the analysis, all samples were stained with 7-AAD staining (BD

BioSciences, 51-68981E) prior to quantitative analysis. The flow cytometry gating strategy is shown in Supplementary Fig. 26. Flow cytometry analysis was performed using a flow cytometer (Attune NxT, Thermo Fisher Scientific), and FlowJo software was used for the analysis of all flow cytometry data.

Flow cytometry-based binding assay

Flow cytometry-based binding assays were performed to assess the relative fluorescence intensity. Tumor cells were incubated with different concentrations of ligand-based switches in the diluent for 1.5 h on ice. After being washed, the cells were stained with anti-Myc tag-FITC for 1 h on ice before data acquisition on a flow cytometer.

ELISA-based binding assay

The binding affinity of various switches to BAFFR/BCMA/TACI antigens was evaluated by ELISA. First, 100 nM of various switches were immobilized on a 96-well ELISA plate at 4 °C, followed by blocking with 5% BSA in Tris-NaCl (pH 8.0) for 2 h at room temperature. After washing with 0.1% Tween-20 in PBS, antigens (BAFFR, BCMA or TACI) at various concentrations were added and incubated for 2 h at 37 °C. The plate was subsequently incubated with HRP-conjugated goat anti-human IgG (BBI, D110150-0100) for 1 h at 37 °C. Following another wash, a substrate solution containing 2,2'-azino-bis(3-ethylbenzothiazoline-6-sulfonate) (ABTS) was added, and the reaction was terminated with 2 M H₂SO₄. Color intensity was measured using a Cytation 5 Cell Imaging Multi-Mode Reader (Agilent Technologies) with excitation at 450 nm. Data analysis was conducted via nonlinear regression using the logarithm (agonist) vs. response model in GraphPad Prism software.

Immunofluorescence analysis of immune synapse formation

A total of 1×10^5 indicated 9E10 CAR-T cells were incubated with various switches (100 nM) for 1 hour at 4 °C. After being washed with 1 mL of cold PBS, the CAR-T cells were resuspended with 5×10^4 indicated tumor cells in RPMI1640 complete media. The samples were then incubated on poly-D-lysine-coated coverslips in an incubator for 1 hour. APRIL- and BAFF-based conventional CAR-T cells were directly co-incubated with tumor cells. Subsequently, the following steps were performed for staining: fixation with 4% neutral formaldehyde to preserve cell morphology, permeabilization with 0.2% Triton X-100 to allow antibody penetration, and blocking with 3% BSA to prevent nonspecific binding. For immunofluorescence, the cells were stained with a primary rabbit anti-human PKC- θ biotin-conjugated antibody (Signalway Antibody, C33151). After being gently washed, the cells were stained with PE-Streptavidin (BioLegend, 405204). To identify the nucleus, the cells were stained with Hoechst (Solarbio, C0031). In the final step, a fluoroshield quencher (Sigma-Aldrich, F6182) was used to prevent fluorescence quenching. The cell-cell conjugates were observed via a laser scanning confocal microscope (A1R, Nikon) with an oil immersion objective (100 \times). The conjugates were analyzed using ImageJ software, and the red region between the tumor and CAR-T cells was identified using a gating strategy.

In vitro cytotoxicity assay

Tumor cells were labeled with the CFSE cell division tracker kit (BioLegend, 423801) following the manufacturer's protocol. To determine the optimal CAR and switch structure, CAR-T cells were co-incubated with target cells at an E:T ratio of 10:1 or 1:1 while maintaining a total cell concentration of 1×10^6 /mL. Different concentrations of switches were added to each well, and the cells were incubated at 37 °C for 24 h in complete RPMI 1640 medium. In the comparison assay, either conventional CAR-T cells or sCAR-T cells with 1 nM switches, were co-cultured with target cells at varying E:T ratios. After incubation, dead cells were excluded by 7-AAD staining. Switch-mediated cytotoxicity was assessed using a flow cytometry by counting the remaining live

target cells, which were identified as 7-AAD⁻CFSE⁺. For the primary patient samples, after incubation, the cells were stained with Pacific Blue anti-human CD3, APC anti-human CD19 and 7-AAD, and live patient tumor cells were identified as 7-AAD⁻hCD3⁺hCD19⁺ cells.

Cytokine release assay

CAR-T cells and target cells were co-cultured at either a 10:1 or 1:1 E:T ratio at 37 °C for 24 h, and switches were added at a concentration of 100 pM. The levels of cytokines secreted into the culture medium were measured using human IL-2 (Thermo Fisher Scientific, 88-7025-88), IFN- γ (Thermo Fisher Scientific, 88-7316-88) and TNF- α (Thermo Fisher Scientific, 88-7346-88) test kits following the manufacturers' protocols. All the tests were conducted in triplicate, and the in vitro data are presented as mean \pm SDs, while in vivo data are presented as mean \pm SEMs.

Western blot

To determine the molecular weight of the CAR, 9E10-IgG4m CAR-T cells or untransduced T cells were co-cultured with Nalm6 or RPMI8226 cells at a 1:1 E:T ratio in complete RPMI 1640 medium containing Myc-BAFF or Myc-APRIL at concentrations of 1/10/100 nM. The co-culture mixture was incubated for 30 minutes, followed by rapid washing twice with ice-cold PBS and lysis with strong lysis buffer containing a protease inhibitor (Mei5bio, MF182-plus-01). The cell lysates were centrifuged at $10,000 \times g$ at 4 °C for 10 minutes, and the supernatants were quantified using a BCA protein assay kit (Elabscience, E-BC-K318-M). Subsequently, 15 μ g of non-reduced whole-cell lysates were loaded onto an 8% SDS-PAGE gel. After the proteins were transferred onto nitrocellulose membranes, the membranes were blocked with 5% non-fat milk and incubated with primary antibodies (anti-human CD3 ζ , Santa Cruz Biotechnology, sc-1239) and secondary antibodies (anti-mouse IgG-HRP, TransGen Biotech, HS201-01) diluted in blocking buffer.

Pharmacokinetics

Female BALB/c mice aged 6 to 8 weeks were purchased from Zhejiang Vital River Laboratory Animal Technology Co., Ltd. Myc-APRIL and Myc-BAFF switches were labeled with IRDye800CW (LI-COR, P/N 928-38040) following the manufacturer's protocol. Female BALB/c mice ($n=3$ /group) received intravenous injections of IRDye800-labeled Myc-APRIL or Myc-BAFF at a dose of 3 nmol per mouse. Blood samples (30 μ L) were collected from the retro-orbital venous plexus of each mouse at 5, 10, and 30 minutes and at 1, 2, 4, 8, and 24 h post-injection. The switch concentrations in the blood samples were determined using a standard curve. Half-life parameters were analyzed via GraphPad Prism analysis software.

Biodistribution

Female NSG mice aged 6–8 weeks were subcutaneously inoculated with 10×10^6 RPMI8226 cells or 5×10^6 Raji cells, and the tumors were allowed to reach 500 mm³ in size before injection. The distribution of intravenous IRDye800-labeled Myc-APRIL and Myc-BAFF switches relative to tumor localization was assessed at 30 min, 6 h, 24 h, and 48 h post-injection.

In vivo efficacy study

All in vivo experimental procedures were approved by the Peking University Shenzhen Graduate School Animal Care and Use Committee and performed according to the national and international guidelines for the ethical treatment of animals. All mice are housed and cared for by trained personnel in a compliant environment. The feeding parameters included ambient temperature 21 °C \pm 1 °C, and humidity 40–70%, dark/light cycle 12/12 (6:00–18:00 light). Female NOD-Prkdc^{scid}Il2rg^{eml}/Smoc (NSG) mice, aged six to eight weeks, were purchased from Shanghai Model Organisms Center, Inc. For the

hematologic tumor model, tumor burden was measured by an IVIS Spectrum (PerkinElmer) and quantified as the average radiance [p/sec/cm²/sr] in the region of interest. Images were acquired within 10 minutes following the intraperitoneal injection of 150 mg/kg D-luciferin (Energy Chemical, E011308). Given the nature of the models, there were no restrictions on tumor size or burden, making direct inferences from external measures unfeasible. Since the tumor cells expressed luciferase, we established a radiance threshold of $\geq 10^{10}$ photons/s/cm²/sr as an upper surrogate limit; however, this was not attained in this study. Animals that experienced a 20% loss of their original body weight were euthanized. In subcutaneous (s.c.) tumor models, tumor volume was measured and calculated using the following formula: Volume = (length \times width²)/2 until it reached a maximum of 20 mm in either length or width or until the total volume reached 2000 mm³, at which point the animals were euthanized. In some cases, this limit has been exceeded by the last day of measurement, and the mice were immediately euthanized.

We initially conducted stress tests in MM and B-ALL tumor models with APRIL- and BAFF-redirected sCAR-T cells, respectively. In the MM model, NSG mice ($n = 4$ /group) received an intravenous (i.v.) inoculation of luciferase-expressing RPMI8226 cells (10×10^6 cells per mouse). Twenty-one days after tumor engraftment, we investigated the dose stress of CAR-T cells and Myc-APRIL. For the CAR-T-cell stress test, the mice were i.v. administered 10×10^6 , 3×10^6 or 1×10^6 9E10-IgG4m CAR-T cells, while the dose of Myc-APRIL was fixed at 1 mg/kg. For the switch stress test, the mice received intraperitoneal (i.p.) injections of 3 mg/kg, 1 mg/kg or 0.3 mg/kg Myc-APRIL, with the CAR-T-cell dose fixed at 10×10^6 cells per mouse. For the B-ALL model, NSG mice ($n = 4$ /group) were inoculated i.v. with luciferase-expressing Nalm6 cells (0.5×10^6 cells per mouse). Three days post-engraftment, we tested the dose-induced stress of CAR-T cells and Myc-BAFF. For the CAR-T-cell stress test, the mice were i.v. injected with 30×10^6 , 10×10^6 or 3×10^6 9E10-IgG4m CAR-T cells, while the dose of Myc-BAFF was fixed at 1 mg/kg. For the switch stress test, the mice received i.p. injections of 3 mg/kg, 1 mg/kg or 0.3 mg/kg Myc-BAFF, with the CAR-T-cell dose fixed at 30×10^6 cells per mouse. Additionally, 50 μ L of blood was drawn two hours after the first administration to determine the serum cytokine concentrations using the IL2/TNF- α /IFN- γ kits according to the manufacturer's standard procedure.

The in vivo efficacy study was designed to compare split-design CAR-T cells with conventional ligand-based CAR-T cells and FDA-approved CAR-T-cell therapies. For the MM model, NSG mice were intravenously (i.v.) inoculated with 1×10^7 luciferized RPMI8226 cells on day 0. On day 21, 10×10^6 CAR-T cells were i.v. infused, followed by intraperitoneal (i.p.) administration of the switches 2 h later, with subsequent dosing every other day for a total of seven doses. In the heterogeneous B-ALL model, a mixture of tumor cells, including luciferase-expressing Nalm6 WT and Nalm6 KO variant cells, was used to establish an immune escape model. Each NSG mouse was i.v. inoculated with 1×10^6 or 0.5×10^6 luciferized Nalm6 mixture on day 0. On day 4, 30×10^6 CAR-T cells were intravenously (i.v.) infused, followed by i.p. administration of the switches 2 h later, which was continued daily for ten doses. For the model of non-Hodgkin lymphoma, NSG mice were s.c. inoculated with 5×10^6 Raji cells or a variant cell mixture on day 0. On day 4, 15 or 30×10^6 CAR-T cells were i.v. infused, followed by i.p. administration of the switches 2 h later, with subsequent dosing every other day for a total of ten doses. To ensure the sustained activity of CAR-T cells in vivo, human IL-7 was injected via the i.p. route at a dose of 100 ng per mouse for a total of 10 injections⁶¹. Tumor volume was measured every three days until the maximal tumor burden was reached. Additionally, 50 μ L of blood was drawn two hours after the first switch to determine serum cytokine concentrations using the IL2/TNF- α /IFN- γ kits, and blood analysis was continued every 4 days for up to five times to access CAR-T cell persistence in peripheral blood.

In vivo synergistic efficacy study

For the dual tumor model of MM and B-ALL, NSG mice were i.v. inoculated with 1×10^7 luciferized RPMI8226 cells on day 0. On day 21, 15×10^6 CAR-T cells (either 9E10-IgG4m or APRIL CAR) were intravenously (i.v.) infused, followed by i.p. administration of Myc-APRIL 2 hours later, with five doses of Myc-APRIL administered daily. On day 28, each NSG mouse received an i.v. inoculation of 0.25×10^6 luciferized Nalm6 cells. Three days later, Myc-BAFF was administered intraperitoneally (i.p.) every day for ten doses. Similarly, on the same day as the first dose of Myc-BAFF, the mice in the conventional CAR-T-cell combination group were intravenously (i.v.) infused with 15×10^6 BAFF CAR-T cells. The tumor burden was monitored using bioluminescence imaging, and peripheral blood was analyzed via flow cytometry at the indicated time points.

Statistical analysis

All the statistical analyzes were performed using GraphPad Prism version 8.4.2 software. *P* values determined by paired two-tailed *t*-tests, one-way or two-way ANOVA multiple comparisons in Dunnett correction, and two-way ANOVA multiple comparisons in Tukey correction. Survival data were analyzed using the log-rank (Mantel-Cox) test. In vitro assay data with experimental replicates are presented as the mean \pm SD, while data from in vivo experiments with biological replicates are presented as the mean \pm SEM.

Reporting summary

Further information on research design is available in the Nature Portfolio Reporting Summary linked to this article.

Data availability

The data are available within the Article, Supplementary Information or Source Data file. Source data are provided with this paper.

References

- Majzner, R. G. & Mackall, C. L. Tumor antigen escape from CAR T-cell Therapy. *Cancer Discov.* **8**, 1219–1226 (2018).
- Shah, N. N. et al. Bispecific anti-CD20, anti-CD19 CAR T cells for relapsed B cell malignancies: a phase 1 dose escalation and expansion trial. *Nat. Med.* **26**, 1569–1575 (2020).
- Spiegel, J. Y. et al. CAR T cells with dual targeting of CD19 and CD22 in adult patients with recurrent or refractory B cell malignancies: a phase 1 trial. *Nat. Med.* **27**, 1419–1431 (2021).
- Mei, H. et al. A bispecific CAR-T cell therapy targeting BCMA and CD38 in relapsed or refractory multiple myeloma. *J. Hematol. Oncol.* **14**, 161 (2021).
- Zah, E. et al. Systematically optimized BCMA/CS1 bispecific CAR-T cells robustly control heterogeneous multiple myeloma. *Nat. Commun.* **11**, 2283 (2020).
- Furqan, F. & Shah, N. N. Multispecific CAR T cells deprive lymphomas of escape via antigen loss. *Annu Rev. Med.* **74**, 279–291 (2023).
- Schneider, D. et al. Trispecific CD19-CD20-CD22-targeting duoCAR-T cells eliminate antigen-heterogeneous B cell tumors in preclinical models. *Sci. Transl. Med.* **13**, eabc6401 (2021).
- Chow, A., Perica, K., Klebanoff, C. A. & Wolchok, J. D. Clinical implications of T cell exhaustion for cancer immunotherapy. *Nat. Rev. Clin. Oncol.* **19**, 775–790 (2022).
- Mulazzani, M. et al. APRIL and BAFF: novel biomarkers for central nervous system lymphoma. *J. Hematol. Oncol.* **12**, 102 (2019).
- Vincent, F. B., Saulep-Easton, D., Figgett, W. A., Fairfax, K. A. & Mackay, F. The BAFF/APRIL system: emerging functions beyond B cell biology and autoimmunity. *Cytokine Growth Factor Rev.* **24**, 203–215 (2013).
- Camviel, N. et al. Both APRIL and antibody-fragment-based CAR T cells for myeloma induce BCMA downmodulation by

- trogocytosis and internalization. *J. Immunother. Cancer* **10**, e005091 (2022).
12. Lee, L. et al. An APRIL-based chimeric antigen receptor for dual targeting of BCMA and TACI in multiple myeloma. *Blood* **131**, 746–758 (2018).
 13. Li, G. et al. TriBAFF-CAR-T cells eliminate B-cell malignancies with BAFFR-expression and CD19 antigen loss. *Cancer Cell Int* **21**, 223 (2021).
 14. Schmidts, A. et al. Rational design of a trimeric APRIL-based CAR-binding domain enables efficient targeting of multiple myeloma. *Blood Adv.* **3**, 3248–3260 (2019).
 15. Wong, D. P. et al. A BAFF ligand-based CAR-T cell targeting three receptors and multiple B cell cancers. *Nat. Commun.* **13**, 217 (2022).
 16. Nicoletti, A. M. et al. Unexpected potency differences between B-cell-activating factor (BAFF) antagonist antibodies against various forms of BAFF: trimer, 60-mer, and membrane-bound. *J. Pharm. Exp. Ther.* **359**, 37–44 (2016).
 17. Cao, Y. et al. Design of switchable chimeric antigen receptor T cells targeting breast cancer. *Angew. Chem. Int Ed. Engl.* **55**, 7520–7524 (2016).
 18. Rodgers, D. T. et al. Switch-mediated activation and retargeting of CAR-T cells for B-cell malignancies. *Proc. Natl Acad. Sci. USA* **113**, E459–E468 (2016).
 19. Viaud, S. et al. Switchable control over in vivo CAR T expansion, B cell depletion, and induction of memory. *Proc. Natl Acad. Sci. USA* **115**, E10898–E10906 (2018).
 20. Cao, Y. J. et al. Switchable CAR-T cells outperformed traditional antibody-redirected therapeutics targeting breast cancers. *ACS Synth. Biol.* **10**, 1176–1183 (2021).
 21. Xiong, W. et al. Immunological synapse predicts effectiveness of chimeric antigen receptor cells. *Mol. Ther.* **26**, 963–975 (2018).
 22. De Munter, S. et al. Nanobody Based Dual Specific CARs. *Int. J. Mol. Sci.* **19**, 403 (2018).
 23. Monks, C. R., Kupfer, H., Tamir, I., Barlow, A. & Kupfer, A. Selective modulation of protein kinase C- θ during T-cell activation. *Nature* **385**, 83–86 (1997).
 24. Leick, M. B. et al. Non-cleavable hinge enhances avidity and expansion of CAR-T cells for acute myeloid leukemia. *Cancer Cell* **40**, 494–508.e495 (2022).
 25. Xiao, Q. et al. Size-dependent activation of CAR-T cells. *Sci. Immunol.* **7**, eabl3995 (2022).
 26. Möckel, T., Basta, F., Weinmann-Menke, J. & Schwarting, A. B cell activating factor (BAFF): structure, functions, autoimmunity and clinical implications in Systemic Lupus Erythematosus (SLE). *Autoimmun. Rev.* **20**, 102736 (2021).
 27. Brudno, J. N. & Kochenderfer, J. N. Toxicities of chimeric antigen receptor T cells: recognition and management. *Blood* **127**, 3321–3330 (2016).
 28. Bossen, C. & Schneider, P. BAFF, APRIL and their receptors: structure, function and signaling. *Semin Immunol.* **18**, 263–275 (2006).
 29. Xu, J. et al. Exploratory trial of a biepitopic CAR T-targeting B cell maturation antigen in relapsed/refractory multiple myeloma. *Proc. Natl Acad. Sci. USA* **116**, 9543–9551 (2019).
 30. Wen, X. et al. Biodistribution, pharmacokinetics, and nuclear imaging studies of ¹¹¹In-labeled rGel/BLYS fusion toxin in SCID mice bearing B cell lymphoma. *Mol. Imaging Biol.* **13**, 721–729 (2011).
 31. Maia, S. et al. Aberrant expression of functional BAFF-system receptors by malignant B-cell precursors impacts leukemia cell survival. *PLoS One* **6**, e20787 (2011).
 32. Novak, A. J. et al. Expression of BCMA, TACI, and BAFF-R in multiple myeloma: a mechanism for growth and survival. *Blood* **103**, 689–694 (2004).
 33. Gauthier, L. et al. Multifunctional natural killer cell engagers targeting NKp46 trigger protective tumor immunity. *Cell* **177**, 1701–1713.e1716 (2019).
 34. Qin, H. et al. Preclinical development of bivalent chimeric antigen receptors targeting both CD19 and CD22. *Mol. Ther. Oncolytics* **11**, 127–137 (2018).
 35. Zhao, L. et al. A novel CD19/CD22/CD3 trispecific antibody enhances therapeutic efficacy and overcomes immune escape against B-ALL. *Blood* **140**, 1790–1802 (2022).
 36. Hamieh, M., Mansilla-Soto, J., Rivière, I. & Sadelain, M. Programming CAR T cell tumor recognition: tuned antigen sensing and logic gating. *Cancer Discov.* **13**, 829–843 (2023).
 37. Kwon, J., et al. Single-cell mapping of combinatorial target antigens for CAR switches using logic gates. *Nat Biotechnol.* **41**, 1593–1605 (2023).
 38. Tousley, A. M. et al. Co-opting signalling molecules enables logic-gated control of CAR T cells. *Nature* **615**, 507–516 (2023).
 39. Li, H.-S. et al. High-performance multiplex drug-gated CAR circuits. *Cancer Cell* **40**, 1294–1305.e1294 (2022).
 40. Yu, S., Yi, M., Qin, S. & Wu, K. Next generation chimeric antigen receptor T cells: safety strategies to overcome toxicity. *Mol. Cancer* **18**, 125 (2019).
 41. Gardner, R. A. et al. Intent-to-treat leukemia remission by CD19 CAR T cells of defined formulation and dose in children and young adults. *Blood* **129**, 3322–3331 (2017).
 42. Parikh, R. H. & Lonial, S. Chimeric antigen receptor T-cell therapy in multiple myeloma: a comprehensive review of current data and implications for clinical practice. *CA Cancer J. Clin.* **73**, 275–285 (2023).
 43. Raje, N. et al. Anti-BCMA CAR T-cell therapy bb2121 in relapsed or refractory multiple myeloma. *N. Engl. J. Med.* **380**, 1726–1737 (2019).
 44. Turtle, C. J. et al. CD19 CAR-T cells of defined CD4⁺:CD8⁺ composition in adult B cell ALL patients. *J. Clin. Invest* **126**, 2123–2138 (2016).
 45. Branella, G. M. & Spencer, H. T. Natural Receptor- and ligand-based chimeric antigen receptors: strategies using natural ligands and receptors for targeted cell killing. *Cells* **11**, 21 (2021).
 46. Dai, H. et al. Bispecific CAR-T cells targeting both CD19 and CD22 for therapy of adults with relapsed or refractory B cell acute lymphoblastic leukemia. *J. Hematol. Oncol.* **13**, 30 (2020).
 47. Abreu, T. R., Fonseca, N. A., Gonçalves, N. & Moreira, J. N. Current challenges and emerging opportunities of CAR-T cell therapies. *J. Control Release* **319**, 246–261 (2020).
 48. Dwivedi, A., Karulkar, A., Ghosh, S., Rafiq, A. & Purwar, R. Lymphocytes in cellular therapy: functional regulation of CAR T Cells. *Front Immunol.* **9**, 3180 (2018).
 49. Nakazawa, Y., et al. Anti-proliferative effects of T cells expressing a ligand-based chimeric antigen receptor against CD116 on CD34(+) cells of juvenile myelomonocytic leukemia. *J. Hematol. Oncol.* **9**, 27(2016).
 50. Ramírez-Chacón, A. et al. Ligand-based CAR-T cell: Different strategies to drive T cells in future new treatments. *Front Immunol.* **13**, 932559 (2022).
 51. Wang, Y. et al. Targeting FLT3 in acute myeloid leukemia using ligand-based chimeric antigen receptor-engineered T cells. *J. Hematol. Oncol.* **11**, 60 (2018).
 52. Lyu, M.-A. et al. The rGel/BLYS fusion toxin specifically targets malignant B cells expressing the BLYS receptors BAFF-R, TACI, and BCMA. *Mol. Cancer Ther.* **6**, 460–470 (2007).
 53. Mackay, F. & Browning, J. L. BAFF: a fundamental survival factor for B cells. *Nat. Rev. Immunol.* **2**, 465–475 (2002).
 54. Nimmanapalli, R. et al. The growth factor fusion construct containing B-lymphocyte stimulator (BLYS) and the toxin rGel induces apoptosis specifically in BAFF-R-positive CLL cells. *Blood* **109**, 2557–2564 (2007).

55. Nowacka, K. H. & Jabłońska, E. Role of the APRIL molecule in solid tumors. *Cytokine Growth Factor Rev.* **61**, 38–44 (2021).
56. Popat, R. et al. Phase 1 first-in-human study of AUTO2, the first chimeric antigen receptor (CAR) T cell targeting APRIL for patients with relapsed/refractory multiple myeloma (RRMM). *Blood* **134**, 3112–3112 (2019).
57. Lee, L. et al. Limited efficacy of APRIL CAR in patients with multiple myeloma indicate challenges in the use of natural ligands for CAR T-cell therapy. *J. Immunother. Cancer* **11**, e006699 (2023).
58. Hudecek, M. et al. Receptor affinity and extracellular domain modifications affect tumor recognition by ROR1-specific chimeric antigen receptor T cells. *Clin. Cancer Res* **19**, 3153–3164 (2013).
59. Hudecek, M. et al. The nonsignaling extracellular spacer domain of chimeric antigen receptors is decisive for in vivo antitumor activity. *Cancer Immunol. Res.* **3**, 125–135 (2015).
60. Liu, D., Zhao, J. & Song, Y. Engineering switchable and programmable universal CARs for CAR T therapy. *J. Hematol. Oncol.* **12**, 69 (2019).
61. Kim, M. Y. et al. A long-acting interleukin-7, rhIL-7-hyFc, enhances CAR T cell expansion, persistence, and anti-tumor activity. *Nat. Commun.* **13**, 3296 (2022).

Acknowledgements

The authors are grateful to all members of the Yu J. Cao group for their technical assistance and helpful discussions. We thank Huazhong University of Science and Technology Union Shenzhen Hospital (Nanshan Hospital) for providing patient samples used in the manuscript. This work was supported by the National Key R&D Program of China (2019YFA0906100 and 2019YFA0904200), the National Natural Science Foundation of China (32171464), and the Shenzhen Science and Technology Innovation Program (JCYJ20180504165501371).

Author contributions

Y.J.C. and S.L. designed the study, analyzed the data and wrote the manuscript; S.L. performed the experiments; L.S. assisted in the in vivo experiments; L.Z. provided the CD19 or CD22 knockout Nalm6 cell lines and assisted in the immunofluorescence analysis; Qiaoru Guo assisted in protein expression; Jun Li provided the T-cell transduction protocols; Z.L. and Z.G. provided the patient samples; and all the authors reviewed the manuscript, approved the final version, and agreed to submit the manuscript for publication.

Competing interests

The Chinese patent “A method to prepare natural ligand-mediated switchable gene-modified immune cells against multiple targets” with the application number CN202010073487.1 is related to the present work. The applicant for the patent is Peking University Shenzhen Graduate School. The authors declare that they have no competing interests.

Additional information

Supplementary information The online version contains supplementary material available at <https://doi.org/10.1038/s41467-024-54150-z>.

Correspondence and requests for materials should be addressed to Yu J. Cao.

Peer review information *Nature Communications* thanks Martin Pule and the other, anonymous, reviewer(s) for their contribution to the peer review of this work. A peer review file is available.

Reprints and permissions information is available at <http://www.nature.com/reprints>

Publisher’s note Springer Nature remains neutral with regard to jurisdictional claims in published maps and institutional affiliations.

Open Access This article is licensed under a Creative Commons Attribution-NonCommercial-NoDerivatives 4.0 International License, which permits any non-commercial use, sharing, distribution and reproduction in any medium or format, as long as you give appropriate credit to the original author(s) and the source, provide a link to the Creative Commons licence, and indicate if you modified the licensed material. You do not have permission under this licence to share adapted material derived from this article or parts of it. The images or other third party material in this article are included in the article’s Creative Commons licence, unless indicated otherwise in a credit line to the material. If material is not included in the article’s Creative Commons licence and your intended use is not permitted by statutory regulation or exceeds the permitted use, you will need to obtain permission directly from the copyright holder. To view a copy of this licence, visit <http://creativecommons.org/licenses/by-nc-nd/4.0/>.

© The Author(s) 2024